Research Article **Open Access**

Qingshan Wang*, Dongyan Shi, Fuzhen Pang, and Qian Liang

Vibrations of Composite Laminated Circular Panels and Shells of Revolution with General Elastic Boundary Conditions via Fourier-Ritz Method

DOI 10.1515/cls-2016-0010
Received Mar 23, 2016; accepted Mar 28, 2016

Abstract: A Fourier-Ritz method for predicting the free vibration of composite laminated circular panels and shells of revolution subjected to various combinations of classical and non-classical boundary conditions is presented in this paper. A modified Fourier series approach in conjunction with a Ritz technique is employed to derive the formulation based on the first-order shear deformation theory. The general boundary condition can be achieved by the boundary spring technique in which three types of liner and two types of rotation springs along the edges of the composite laminated circular panels and shells of revolution are set to imitate the boundary force. Besides, the complete shells of revolution can be achieved by using the coupling spring technique to imitate the kinematic compatibility and physical compatibility conditions of composite laminated circular panels at the common meridian with $\theta = 0$ and 2π. The comparisons established in a sufficiently conclusive manner show that the present formulation is capable of yielding highly accurate solutions with little computational effort. The influence of boundary and coupling restraint parameters, circumference angles, stiffness ratios, numbers of layer and fiber orientations on the vibration behavior of the composite laminated circular panels and shells of revolution are also discussed.

Keywords: Fourier-Ritz method; Free vibration; Composite laminated materials; Circular panels and shells of revolution; General Elastic Boundary

***Corresponding Author: Qingshan Wang:** College of Mechanical and Electrical Engineering, Harbin Engineering University, Harbin, 150001, PR China; Email: wangqingshanxlz@hotmail.com; Tel.: +86-451-82519797

Dongyan Shi, Qian Liang: College of Mechanical and Electrical Engineering, Harbin Engineering University, Harbin, 150001, PR China

Fuzhen Pang: College of Shipbuilding Engineering, Harbin Engineering University, Harbin, 150001, PR China

1 Introduction

The composite laminated circular panels and shells of revolution are widely used as elementary structural components in modern aerospace structures, missiles, naval vehicles and other areas of engineering. These structural elements are commonly subjected to various forms of dynamic loadings in their service life and therefore, the knowledge of their vibration characteristics is of crucial importance from the standpoint of the practical design. However, achieving an accurate and unified vibration solution for composite laminated circular panels and shells of revolution with arbitrary boundary conditions remains an extremely challenging task both analytically and numerically due to the complicated effects involving the transverse shear and normal deformations, coupled material behaviors and non-zero curvatures, etc. The development of relevant theoretical methodologies and numerical modeling for composite laminated circular panels and shells of revolution has thus received considerable attention from the research community. This paper is concerned with the theoretical development and an efficient unified method for free vibration analyses of composite laminated circular panels and shells of revolution based on the first-order shear deformation theory.

In the last decades, a large quantity of research efforts have been devoted to the vibration analysis of composite laminated circular panels and shells of revolution in the literature. Jin *et al.* [1, 2] applied the modified Fourier method to predict the vibration characteristics of moderately thick composite spherical dome and thin shallow shells with general boundary conditions. Later, his [3] group extended the Chebyshev–Ritz method to study the free vibration analysis of spherical panels with general boundary condition. Qu *et al.* [4] analyzed the free and forced vibrations of composite laminated shells of revolution including cylindrical shell, conical shell and spherical shell, in which a modified variational principle in conjunction with a multi-segment partitioning technique was employed to derive the formulation based on the first-order

shear deformation theory. The static and free vibration analysis of laminated shells is performed by radial basis functions collocation, according to a layerwise deformation theory by Ferreira *et al.* [5, 6]. A general survey and comparison for variety of simply supported shallow spherical, cylindrical, plate and saddle panels in rectangular planform was made by Chern and Chao [7]. Free vibration of simply supported laminated spherical panels with random material properties was reported by Singh *et al.* [8] based on the high-order shear deformation shallow theory. The free vibration of composite spherical shell cap with and without a cutout is investigated by Ram and Babu [9] using the finite element method based on a higher-order shear deformation theory. Wu *et al.* [10] performed the natural frequencies and forced responses of thin laminated composite shells of general form by using a high-order curved shell finite element. The free vibration response of doubly-curved anisotropic laminated composite shells is presented by Fazzolari and Carrera [11] using the hierarchical trigonometric Ritz formulation (HTRF). Qatu [12, 13] presented accurate equations which include shells with a pre-twist and accurate force and moment resultants for free vibration of laminated composite deep, thick shells with some selected calssical boundary conditions. Kioua and Mirza [14] presented a simple and efficient method for the static analysis of shallow shells including spherical panels under mechanical, thermal, and piezoelectric fields with classical boundary conditions. Lal *et al.* [15] investigated the nonlinear bending behaviour of laminated composite spherical shell panel with system randomness subjected to hygro-thermo-mechanical loading by using the higher order shear deformation theory and stochastic C^0 nonlinear finite element method. Lee and Chung [16] applied the finite element model for vibrating laminated spherical shell panels with delamination around a central cutout based on the third-order shear deformation theory of Sanders. Mantari *et al.* [17] preseneted a exact solution for static and dynamic analysis of laminated composite and sandwich cylindrical and spherical shells and plates with simply supported boundary conditions based on the new higher order shear deformation theory. Garg *et al.* [18] presented a closed-form formulation of two-dimensional (2D) higher-order shear deformation theories (HOSTs) for the free vibration analysis of simply supported cross-ply laminated composite and sandwich doubly curved shells. Panda and Singh [19, 20] analyzed the nonlinear free vibration behaviour of thermally post-buckled laminated composite spherical shallow shell panel with claaical boundary condition by using the nonlinear finite element approach based on the higher order shear deformation theory (HSDT). Birman *et al.* [21] presented a closed form solution for axisymmetric dynamics of spherical shells reinforced by meridional and circumferential stiffeners with classical boundary conditions. Dasgupta and Huang [22] developed a layer-wise theory for free vibrations of thick composite spherical panels based on the finite element method. Panda and Mahapatra [23] used the higher order shear deformation theory and nonlinear finite element method to investigate the nonlinear free vibration behavior of laminated composite shallow shell with classical boundary conditions.

As is clear from the above literature reviews, the existing works exist two defects: Firstly, most of the existing methods just can be used to achieve the spherical panels and dome with classical boundary condition; Secondly, the exsting results about the titled problems is confined to the composite laminate spherical panels and dome. However, in the practical engineering, the boundary condition of the work strtures can't always be classical in nature. In addition, the revolution axis of rotation may not coincide with the spherical coordinate center and it occurs a shift between them. Unfortunately, there is a considerable lack of corresponding information to deal with the vibration analysis of composite laminated circular panels and shells of revolution subjected to non-classical edge boundary conditions. Thus, it is desirable to develop a unified, efficient method which is capable of dealing with composite laminated circular panels and shells of revolution subjected to general elastic restraints. Recently, the improved Fourier series was proposed in 2000 by Li [24–26] to solve the free vibration of beams with general boundary conditions. Later, the method fast extended to cope with other structures (*i.e.* beams, plates, shells and coupled structures) by the Du [27–30], Jin [31–46], Wang *et al.* [47–52] in the last ten years due to the superiority compared with other methods. The detailed theoretical analyses and mathematical principle can been seen in Refs [24–26]. The main focus of this work is to complement the vibration studies of composite laminated circular panels and shells of revolution with general elastic restraints and develop a unified and sufficiently accurate analytical method to provide some useful results of the titled problem which may be used for benchmarking by future researchers. The first-order shear deformation shell theory is adopted to formulate the theoretical model. In summary, there are five merits in present work: Firstly, regardless of boundary conditions, the admissible function of the composite laminated circular panels and shells of revolution is obtained by the improved Fourier series which consists of a superposition of the standard cosine Fourier series and several auxiliary functions introduced to remove any potential discontinuous of the original displacement and its derivatives at the

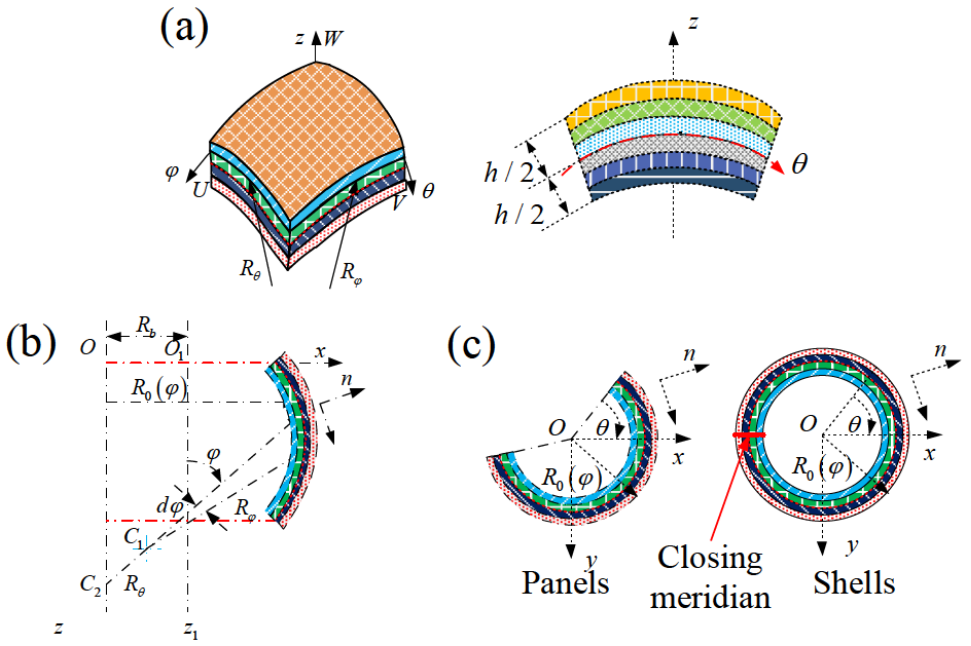

Figure 1: The geometric parameters and coordinate system of a composite laminated shell: (a) the differential element of the composite laminated shell; (b) the spherical shell coordinate system; (c) circumferential section of the composite laminated shell.

boundaries; Secondly, the general elastic restraints can be achieved by the boundary spring technique in which three types of liner and two types of rotation springs along the edges of the circular panels and shells of revolution are used to imitate the boundary condition. Thirdly, the complete shells of revolution can be achieved by using the coupling spring technique to imitate the kinematic compatibility and physical compatibility conditions of laminated circular panels at the common meridian with $\theta = 0$ and 2π. Then, the present solutions enables rapid convergence, high reliability and accuracy since the unknown coefficients appearing in the admissible function are determined by using the Ritz procedure, compared with other contributions. Lastly, Numerous new free vibration results for the composite laminated circular panels and shells of revolution with different lamination schemes and elastic restraints are presented and the influence of boundary and coupling restraint parameters, circumference angles, stiffness ratios, numbers of layer and fiber orientations on the vibration behavior of the composite laminated circular panels and shells of revolution are also presented, which can be served as benchmark data for the designers and engineers to avoid the unpleasant, inefficient and structurally damaging resonant.

2 Theoretical formulations

2.1 Description of the model

The basic configuration of the problem considered here is a composite laminated doubly-curved shell as shown in Fig. 1. An orthogonal curvilinear coordinate system (φ, θ, z) is fixed in the reference surface which usually refers to the middle surface of the shell. The displacements of the shell in the meridional φ, circumferential θ and radial z directions are denoted by u, v and w, respectively. The angle formed by the external normal **n** to the reference surface and the axis of rotation Oz, or the geometric axis O_1z_1 of the meridian curve, is defined as the meridional angle φ and the angle between the radius of the parallel circle and the x axis is designated as the circumferential angle θ as shown in Fig. 1. The position of an arbitrary point within the shell is decided by $\varphi_0 < \varphi < \varphi_1$, $0 < \theta < \phi$ and $h/2 < z < h/2$. The horizontal radius is designated as R_0, and the radii of curvature in the meridional and circumferential directions are respectively represented by R_φ, R_θ. The included angle between the material coordinate of the k'th layer and the φ-axis of the shell is denoted by α, and the distances from the undersurface and the top surface of the layer to the reference surface are assigned as z_k and z_{k+1}, respectively. For a surface of revolution with a circu-

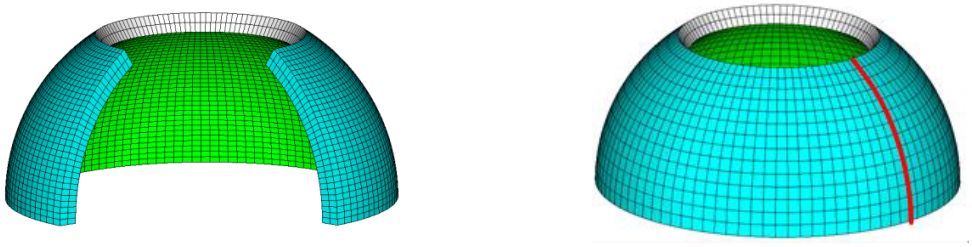

(a) Spherical panel and Spherical dome

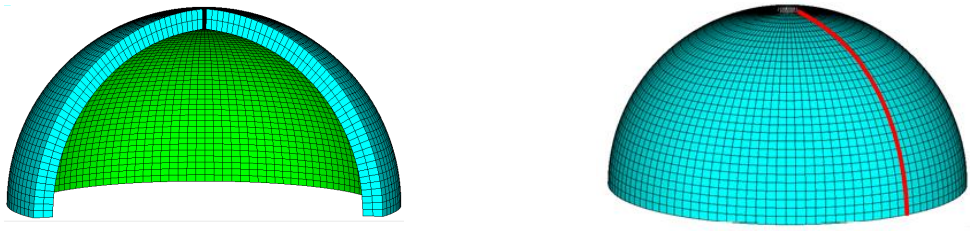

(b) Spherical cap

(c) Toro-circular panel and Circular toroid (R_b=-1.5)

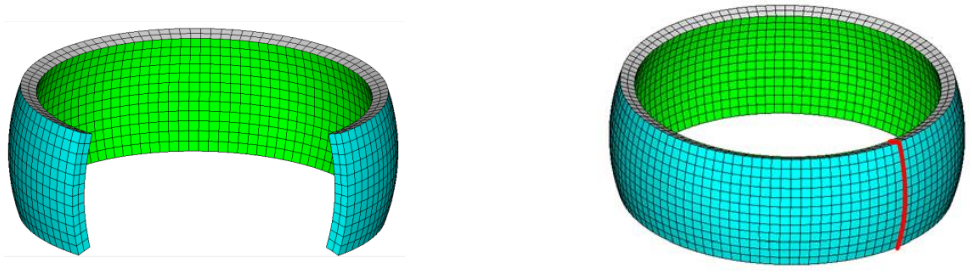

(d) Toro-circular panel and Circular toroid (R_b=1.5)

Figure 2: Composite laminated circular panels and shells of revolution structures.

lar curved meridian, they are respectively expressed as:

$$R_0 = R\sin\varphi + R_b, \quad R_\theta = R_0/\sin\varphi, \quad R_\varphi = R \qquad (1)$$

where R is the constant radius of the circular meridian of the shell. R_b is the distance between the axis of rotation Oz and the geometric axis of the meridian O_1z_1. Fig. 2 shows the examined composite laminated circular panels and shells of revolution structures for the verification of the accuracy and versatility of the proposed approach.

The spherical panel and dome is generated as a special case of the considered panels shells of revolution structures, when $R_b = 0$, as diagramed in Fig. 2(a) and by setting $\varphi_0 = 0$, the spherical cap is obtained as illustrated in Fig. 2(b). It is worth noting that, by setting the $R_b \neq 0$, the panels and shells of revolution structures are transformed to the Toro-circular panel and Circular toroid, as shown in Fig. 2(c) ($R_b < 0$) and 2(d) ($R_b > 0$).

2.2 Kinematic relations and stress resultants

Consistent with the assumptions of the moderately thick shell theory reported above, the displacement field considered in this study is that of the first order shear deformation theory and can be put in the following form [53–55]:

$$U(\varphi, \theta, z, t) = u_0(\varphi, \theta, t) + z\psi_\varphi(\varphi, \theta, t) \tag{2a}$$

$$V(\varphi, \theta, z, t) = v_0(\varphi, \theta, t) + z\psi_\theta(\varphi, \theta, t) \tag{2b}$$

$$W(\varphi, \theta, z, t) = w_0(\varphi, \theta, t) \tag{2c}$$

where u_0, v_0 and w denote the displacements of corresponding point on the reference surface in the φ, θ and z directions, respectively. ψ_{varphi} and ψ_{theta} are the rotations of the normal to the reference surface about the θ and φ direction, respectively, and t is the time. Relationships between strains and displacements along the shell reference (middle) surface ($z = 0$) are represented by the following:

$$\begin{aligned}
&\varepsilon_\varphi^0 = \frac{1}{R_\varphi}\left(\frac{\partial u_0}{\partial \varphi} + w_0\right) \quad \varepsilon_\theta^0 = \frac{1}{R_0}\left(\frac{\partial v_0}{\partial \theta} + u_0\cos\varphi + w_0\sin\varphi\right), \\
&\gamma_{\varphi z}^0 = \frac{1}{R_\varphi}\left(\frac{\partial w_0}{\partial \varphi} - u_0\right) + \psi_\varphi, \quad \gamma_{\theta z}^0 = \frac{1}{R_0}\left(\frac{\partial w_0}{\partial \theta} - v_0\sin\varphi\right) + \psi_\theta \\
&\gamma_{\varphi\theta}^0 = \frac{1}{R_\varphi}\frac{\partial v_0}{\partial \varphi} + \frac{1}{R_0}\left(\frac{\partial u_0}{\partial \theta} - v_0\cos\varphi\right) \kappa_\varphi = \frac{1}{R_\varphi}\frac{\partial \psi_\varphi}{\partial \varphi}, \quad \kappa_\theta = \frac{1}{R_0}\left(\frac{\partial \psi_\theta}{\partial \theta} + \psi_\varphi\cos\varphi\right), \\
&\kappa_{\varphi\theta} = \frac{1}{R_\varphi}\frac{\partial \psi_\theta}{\partial \varphi} + \frac{1}{R_0}\left(\frac{\partial \psi_\varphi}{\partial \theta} - \psi_\theta\cos\varphi\right)
\end{aligned} \tag{3}$$

The constitutive equations relating the force and moment resultants to strains and curvatures of the reference surface are given in the matrix form:

$$\begin{bmatrix} N_\varphi \\ N_\theta \\ N_{\varphi\theta} \\ M_\varphi \\ M_\theta \\ M_{\varphi\theta} \end{bmatrix} = \begin{bmatrix} A_{11} & A_{12} & A_{16} & B_{11} & B_{12} & B_{16} \\ A_{12} & A_{22} & A_{26} & B_{12} & B_{22} & B_{26} \\ A_{16} & A_{26} & A_{66} & B_{16} & B_{26} & B_{66} \\ B_{11} & B_{12} & B_{16} & D_{11} & D_{12} & D_{16} \\ B_{12} & B_{22} & B_{26} & D_{12} & D_{22} & D_{26} \\ B_{16} & B_{26} & B_{66} & D_{16} & D_{26} & D_{66} \end{bmatrix} \begin{bmatrix} \varepsilon_\varphi^0 \\ \varepsilon_\theta^0 \\ \gamma_{\varphi\theta}^0 \\ \kappa_\varphi \\ \kappa_\theta \\ \kappa_{\varphi\theta} \end{bmatrix}, \quad \begin{bmatrix} Q_\varphi \\ Q_\theta \end{bmatrix} = \kappa \begin{bmatrix} A_{55} & A_{45} \\ A_{45} & A_{44} \end{bmatrix} \begin{bmatrix} \gamma_{\varphi z}^0 \\ \gamma_{\theta z}^0 \end{bmatrix} \tag{4}$$

where N_φ, N_θ and $N_{\varphi\theta}$ are the in-plane force resultants, M_φ, M_θ and $M_{\varphi\theta}$ are moment resultants, Q_φ, Q_θ are transverse shear force resultants. κ is the shear correction factor, which is usually selected as $\kappa = 5/6$. A_{ij}, B_{ij} and D_{ij} (i, $j = 1, 2$ and 6) are the extensional, extensional-bending coupling, bending stiffness, and they are respectively expressed as

$$A_{ij} = \sum_{k=1}^{N} \overline{Q}_{ij}^k (Z_{k+1} - Z_k) \, (i, j = 1, 2, 4, 5, 6) \tag{5a}$$

$$B_{ij} = \frac{1}{2}\sum_{k=1}^{N} \overline{Q}_{ij}^k \left(Z_{k+1}^2 - Z_k^2\right) (i, j = 1, 2, 6) \tag{5b}$$

$$D_{ij} = \frac{1}{3}\sum_{k=1}^{N} \overline{Q}_{ij}^k \left(Z_{k+1}^3 - Z_k^3\right) (i, j = 1, 2, 6) \tag{5c}$$

where $\overline{Q}_{ij}^k$ ($i, j = 1, 2, 4 - 6$) are the lamina stiffness coefficients, and their detailed information are shown in Appendix A.

The strain energy (U_s) of the composite laminated circular panels and shells of revolution during vibration can be define as

$$U_s = \frac{1}{2}\int\int\int_V \left\{ \begin{matrix} N_\varphi\varepsilon_\varphi^0 + N_\theta\varepsilon_\theta^0 + N_{\varphi\theta}\gamma_{\varphi\theta}^0 + M_\varphi\kappa_\varphi \\ +M_\theta\kappa_\theta + +M_{\varphi\theta}\kappa_{\varphi\theta} + Q_\varphi\gamma_{\varphi z}^0 + Q_\theta\gamma_{\theta z}^0 \end{matrix} \right\} R_0 R_\varphi \, d\varphi \, d\theta \, dz \tag{6}$$

Substituting Eqs. (3) and (4) into Eq. (6), the strain energy expression of the structure can be written in terms of middle surface displacements and rotations. For convenience, the strain energy expression is divided into three components *i.e.* $U = U_S + U_B + U_{BS}$, where U_S, U_B and U_{BS} indicate Stretching, Bending and Bending–Stretching coupling energy expressions, respectively.

$$U_S = \frac{1}{2}\int_{\varphi_0}^{\varphi_1}\int_{0}^{\phi}\left\{\begin{array}{l} A_{11}\frac{1}{R_\varphi^2}\left(\frac{\partial u_0}{\partial\varphi}+w_0\right)^2 + A_{22}\frac{1}{R_0^2}\left(\frac{\partial v_0}{\partial\theta}+u_0\cos\varphi+w_0\sin\varphi\right)^2 \\ +\kappa A_{55}\left(\frac{1}{R_\varphi}\left(\frac{\partial w_0}{\partial\varphi}-u_0\right)+\psi_\varphi\right)^2 + \kappa A_{44}\left(\frac{1}{R_0}\left(\frac{\partial w_0}{\partial\theta}-v_0\sin\varphi\right)+\psi_\theta\right)^2 \\ +A_{66}\left(\frac{1}{R_\varphi}\frac{\partial v_0}{\partial\varphi}+\frac{1}{R_0}\left(\frac{\partial u_0}{\partial\theta}-v_0\cos\varphi\right)\right)^2 \\ +2A_{12}\frac{1}{R_0R_\varphi}\left(\frac{\partial u_0}{\partial\varphi}+w_0\right)\left(\frac{\partial v_0}{\partial\theta}+u_0\cos\varphi+w_0\sin\varphi\right) \\ +2A_{16}\frac{1}{R_\varphi}\left(\frac{\partial u_0}{\partial\varphi}+w_0\right)\left(\frac{1}{R_\varphi}\frac{\partial v_0}{\partial\varphi}+\frac{1}{R_0}\left(\frac{\partial u_0}{\partial\theta}-v_0\cos\varphi\right)\right) \\ +2A_{26}\frac{1}{R_0}\left(\frac{\partial v_0}{\partial\theta}+u_0\cos\varphi+w_0\sin\varphi\right)\left(\frac{1}{R_\varphi}\frac{\partial v_0}{\partial\varphi}+\frac{1}{R_0}\left(\frac{\partial u_0}{\partial\theta}-v_0\cos\varphi\right)\right) \\ 2\kappa A_{45}\left(\frac{1}{R_\varphi}\left(\frac{\partial w_0}{\partial\varphi}-u_0\right)+\psi_\varphi\right)\left(\frac{1}{R_0}\left(\frac{\partial w_0}{\partial\theta}-v_0\sin\varphi\right)+\psi_\theta\right) \end{array}\right\} R_0R_\varphi d\varphi d\theta \tag{7}$$

$$U_{bs} = \frac{1}{2}\int_{\varphi_0}^{\varphi_1}\int_{0}^{\phi}\left\{\begin{array}{l} 2B_{11}\frac{1}{R_\varphi^2}\left(\frac{\partial u_0}{\partial\varphi}+w_0\right)\left(\frac{\partial\psi_\varphi}{\partial\varphi}\right) + 2B_{12}\frac{1}{R_0R_\varphi}\left(\frac{\partial u_0}{\partial\varphi}+w_0\right)\left(\frac{\partial\psi_\theta}{\partial\theta}+\psi_\varphi\cos\varphi\right) \\ +2B_{16}\frac{1}{R_\varphi}\left(\frac{\partial u_0}{\partial\varphi}+w_0\right)\left(\frac{1}{R_\varphi}\frac{\partial\psi_\theta}{\partial\varphi}+\frac{1}{R_0}\left(\frac{\partial\psi_\varphi}{\partial\theta}-\psi_\theta\cos\varphi\right)\right) \\ +2B_{12}\frac{1}{R_0R_\varphi}\left(\frac{\partial v_0}{\partial\theta}+u_0\cos\varphi+w_0\sin\varphi\right)\left(\frac{\partial\psi_\varphi}{\partial\varphi}\right) \\ +2B_{22}\frac{1}{R_0^2}\left(\frac{\partial v_0}{\partial\theta}+u_0\cos\varphi+w_0\sin\varphi\right)\left(\frac{\partial\psi_\theta}{\partial\theta}+\psi_\theta\cos\varphi\right) \\ +2B_{26}\frac{1}{R_0}\left(\frac{\partial v_0}{\partial\theta}+u_0\cos\varphi+w_0\sin\varphi\right)\left(\frac{1}{R_\varphi}\frac{\partial\psi_\theta}{\partial\varphi}+\frac{1}{R_0}\left(\frac{\partial\psi_\varphi}{\partial\theta}-\psi_\theta\cos\varphi\right)\right) \\ +2B_{16}\frac{1}{R_\varphi}\left(\frac{1}{R_\varphi}\frac{\partial v_0}{\partial\varphi}+\frac{1}{R_0}\left(\frac{\partial u_0}{\partial\theta}-v_0\cos\varphi\right)\right)\left(\frac{\partial\psi_\varphi}{\partial\varphi}\right) \\ +2B_{26}\frac{1}{R_0}\left(\frac{1}{R_\varphi}\frac{\partial v_0}{\partial\varphi}+\frac{1}{R_0}\left(\frac{\partial u_0}{\partial\theta}-v_0\cos\varphi\right)\right)\left(\frac{\partial\psi_\theta}{\partial\theta}+\psi_\varphi\cos\varphi\right) \\ +2B_{66}\left(\frac{1}{R_\varphi}\frac{\partial v_0}{\partial\varphi}+\frac{1}{R_0}\left(\frac{\partial u_0}{\partial\theta}-v_0\cos\varphi\right)\right)\left(\frac{1}{R_\varphi}\frac{\partial\psi_\theta}{\partial\varphi}+\frac{1}{R_0}\left(\frac{\partial\psi_\varphi}{\partial\theta}-\psi_\theta\cos\varphi\right)\right) \end{array}\right\} R_0R_\varphi d\varphi d\theta \tag{8}$$

$$U_b = \frac{1}{2}\int_{\varphi_0}^{\varphi_1}\int_{0}^{\psi}\left\{\begin{array}{l} +2D_{12}\frac{1}{R_0R_\varphi}\left(\frac{\partial\psi_\varphi}{\partial\varphi}\right)\left(\frac{\partial\psi_\theta}{\partial\theta}+\psi_\varphi\cos\varphi\right) \\ +D_{11}\frac{1}{R_\varphi^2}\left(\frac{\partial\psi_\varphi}{\partial\varphi}\right)^2 + D_{22}\frac{1}{R_0^2}\left(\frac{\partial\psi_\theta}{\partial\theta}+\psi_\varphi\cos\varphi\right)^2 \\ +D_{66}\left(\frac{1}{R_\varphi}\frac{\partial\psi_{theta}}{\partial\varphi}+\frac{1}{R_0}\left(\frac{\partial\psi_\varphi}{\partial\theta}-\psi_\theta\cos\varphi\right)\right)^2 \\ +2D_{16}\frac{1}{R_\varphi}\left(\frac{\partial\psi_\varphi}{\partial\varphi}\right)\left(\frac{1}{R_\varphi}\frac{\partial\psi_\theta}{\partial\varphi}+\frac{1}{R_0}\left(\frac{\partial\psi_\varphi}{\partial\theta}-\psi_\theta\cos\varphi\right)\right) \\ +2D_{26}\frac{1}{R_0}\left(\frac{\partial\psi_\theta}{\partial\theta}+\psi_\varphi\cos\varphi\right)\left(\frac{1}{R_\varphi}\frac{\partial\psi_\theta}{\partial\varphi}+\frac{1}{R_0}\left(\frac{\partial\psi_\varphi}{\partial\theta}-\psi_\theta\cos\varphi\right)\right) \end{array}\right\} R_0R_\varphi d\varphi d\theta \tag{9}$$

The corresponding kinetic energy (T) function of the composite laminated circular panels and shells of revolution can be given as:

$$T = \frac{1}{2}\int_{\varphi_0}^{\varphi_1}\int_{0}^{\theta}\int_{-h/2}^{h/2}\rho\left[\left(\frac{\partial U}{\partial t}\right)^2+\left(\frac{\partial V}{\partial t}\right)^2+\left(\frac{\partial W}{\partial t}\right)^2\right]\left(1+\frac{z}{R_\varphi}\right)\left(1+\frac{z}{R_\theta}\right)R_0R_\varphi d\varphi d\theta dz \tag{10}$$

$$\frac{1}{2}\int_{\varphi_0}^{\varphi_1}\int_{0}^{\theta}\left\{\begin{array}{l} I_0\left[\left(\frac{\partial u_0}{\partial t}\right)^2+\left(\frac{\partial v_0}{\partial t}\right)^2+\left(\frac{\partial w_0}{\partial t}\right)^2\right]+2I_1\left(\frac{\partial u_0}{\partial t}\frac{\partial\psi_\varphi}{\partial t}+\frac{\partial v_0}{\partial t}\frac{\partial\psi_\theta}{\partial t}\right) \\ +I_2\left[\left(\frac{\partial\psi_\varphi}{\partial t}\right)^2+\left(\frac{\partial\psi_\theta}{\partial t}\right)^2\right] \end{array}\right\} R_0R_\varphi d\varphi d\theta dz$$

where

$$(I_0\ I_1\ I_2) = \int_{-h/2}^{h/2}\rho(z)\left(1+\frac{z}{R_\varphi}\right)\left(1+\frac{z}{R_\theta}\right)\left(1,z^1,z^2\right)dz \tag{11}$$

Table 1: The corresponding spring stiffness values for general boundary conditions.

Edges	BC	Essential conditions	Corresponding spring stiffness values				
			Γ_u	Γ_v	Γ_w	Γ_φ	Γ_θ
φ = constant	F	$N_\varphi = N_{\varphi\theta} = Q_\varphi = M_\varphi = M_{\varphi\theta} = 0$	0	0	0	0	0
	C	$U = V = W = \Phi_\varphi = \Phi_\theta = 0$	10^8D	10^8D	10^8D	10^8D	10^8D
	S	$U = V = W = M_\varphi = \Phi_\theta = 0$	10^8D	10^8D	10^8D	0	10^8D
	SD	$N_\varphi = V = W = M_\varphi = \Phi_\theta = 0$	0	10^8D	10^8D	0	0
	E^1	$U = V = W \neq 0; \Phi_\varphi = \Phi_\theta = 0$	10^2D	10^2D	10^2D	10^8D	10^8D
	E^2	$U = V = W = 0; \Phi_\varphi = \Phi_\theta \neq 0$	10^8D	10^8D	10^8D	10^2D	10^2D
	E^3	$N_\varphi = N_{\varphi\theta} = Q_\varphi = M_\varphi = M_{\varphi\theta} \neq 0$	10^2D	10^2D	10^2D	10^2D	10^2D
θ = constant	F	$N_\varphi = N_{\varphi\theta} = Q_\varphi = M_\varphi = M_{\varphi\theta} = 0$	0	0	0	0	0
	C	$U = V = W = \Phi_\varphi = \Phi_\theta = 0$	10^8D	10^8D	10^8D	10^8D	10^8D
	S	$U = V = W = \Phi_\varphi = M_\theta = 0$	10^8D	10^8D	10^8D	10^8D	0
	SD	$U = N_{\varphi\theta} = W = M_\varphi = M_{\varphi\theta} = 0$	10^8D	0	10^8D	0	0
	E^1	$U = V = W \neq 0; \Phi_\varphi = \Phi_\theta = 0$	10^2D	10^2D	10^2D	10^8D	10^8D
	E^2	$U = V = W = 0; \Phi_\varphi = \Phi_\theta \neq 0$	10^8D	10^8D	10^8D	10^2D	10^2D
	E^3	$N_\varphi = N_{\varphi\theta} = Q_\varphi = M_\varphi = M_{\varphi\theta} \neq 0$	10^2D	10^2D	10^2D	10^2D	10^2D

Since the main focus of this paper is to develop a unified solution for the vibration analysis of the composite laminated circular panels and shells of revolution with general boundary conditions, thus, in order to satisfy the request, the artificial spring boundary technique is adopted here. In this technique, five groups of boundary restraining springs are arranged at all sides of the circular panels and shells of revolution to separately simulate the general boundary conditions. Then the equations describing general elastic supported composite laminated circular panels and shells of revolution can be written as follows:

$$\text{At } \varphi = \varphi 0, \quad k^u_{\varphi 0} U = N_\varphi,\ k^u_{\varphi 0} V = N_{\varphi\theta},\ k^w_{\varphi 0} W = Q_\varphi,\ K^\varphi_{\varphi 0} \Phi_\varphi = M_\varphi,\ K^\theta_{\varphi 0} \Phi_\theta = M_{\varphi\theta} \tag{12}$$

$$\text{At } \varphi = \varphi 1, \quad k^u_{\varphi 1} U = -N_\varphi,\ k^u_{\varphi 1} V = -N_{\varphi\theta},\ k^w_{\varphi 1} W = -Q_\varphi,\ K^\varphi_{\varphi 1} \Psi_\varphi = -M_\varphi,\ K^\theta_{\varphi 1} \Psi_\theta = -M_{\varphi\theta} \tag{13}$$

$$\text{At } \theta = 0, \quad k^u_{\theta 0} U = N_\theta,\ k^u_{\theta 0} V = N_{\varphi\theta},\ k^w_{\theta 0} W = Q_\theta,\ K^\varphi_{\theta 0} \Psi_\varphi = M_\theta,\ K^\theta_{\theta 0} \Psi_\theta = M_{\varphi\theta} \tag{14}$$

$$\text{At } \theta = \phi, \quad k^u_{\theta 0} U = -N_\theta,\ k^u_{\theta 0} V = -N_{\varphi\theta},\ k^w_{\theta 0} W = -Q_\theta,\ K^\varphi_{\theta 0} \Psi_\varphi = -M_\theta,\ K^\theta_{\theta 0} \Psi_\theta = -M_{\varphi\theta} \tag{15}$$

Thus, as one merit of the present study, the unified treatment in dealing with general boundary conditions for the panels can be achieved by assigning the stiffness of the boundary springs with various values. For example the free boundary condition can be readily obtained by setting the spring coefficients to zeros, and the clamped boundary can be obtained by assigning the springs' stiffness to infinity. Table 1 gives the corresponding spring stiffness values for the considered boundaries. Therefore, the potential energy U_{sp} stored in the boundary springs is given as:

$$\begin{aligned} U_{sp} = {} & \frac{1}{2} \int_{-\frac{h}{2}}^{\frac{h}{2}} \int_0^{\phi} \left\{ \begin{array}{l} \left[k^u_{\varphi 0} u_0^2 + k^v_{\varphi 0} v_0^2 + k^w_{\varphi 0} w_0^2 + K^\varphi_{\varphi 0} \psi_\varphi^2 + K^\theta_{\varphi 0} \psi_\theta^2 \right]_{\varphi=\varphi 0} \\ \left[k^u_{\varphi 1} u_0^2 + k^v_{\varphi 1} v_0^2 + k^w_{\varphi 1} w_0^2 + K^\varphi_{\varphi 1} \psi_\varphi^2 + K^\theta_{\varphi 1} \psi_\theta^2 \right]_{\varphi=\varphi 1} \end{array} \right\} R_0 d\theta dz \\ & + \frac{1}{2} \int_{-\frac{h}{2}}^{\frac{h}{2}} \int_{\varphi 0}^{\varphi 1} \left\{ \begin{array}{l} \left[k^u_{\theta 0} u_0^2 + k^v_{\theta 0} v_0^2 + k^w_{\theta 0} w_0^2 + K^\varphi_{\theta 0} \psi_\varphi^2 + K^\theta_{\theta 0} \psi_\theta^2 \right]_{\theta=0} \\ \left[k^u_{\theta 1} u_0^2 + k^v_{\theta 1} v_0^2 + k^w_{\theta 1} w_0^2 + K^\varphi_{\theta 1} \psi_\varphi^2 + K^\theta_{\theta 1} \psi_\theta^2 \right]_{\theta=\phi} \end{array} \right\} R_\varphi d\varphi dz \end{aligned} \tag{16}$$

In addition to the external boundary conditions, the kinematic and physical compatibility should be satisfied at the common meridian with $\theta = 0$ and 2π, if a complete shell of revolution is considered. The kinematic compatibility conditions include the continuity of displacements. The physical compatibility conditions can only be the five continuous

conditions for the generalized stress resultants [53–55]. Thus, as shown in Fig. 1 (d), to consider the complete shell of revolution characterized by $\phi = 2\pi$, it is necessary to implement the kinematic and physical compatibility conditions between the two computational meridians of $\theta = 0$ and $\phi = 2\pi$.

The kinematic compatibility conditions:

$$\begin{aligned} &u_0(\varphi,0,t) = u_0(\varphi,\phi,t),\ v_0(\varphi,0,t) = v_0(\varphi,\phi,t),\ w_0(\varphi,0,t) = w_0(\varphi,\phi,t) \\ &\psi_\varphi(\varphi,0,t) = \psi_\varphi(\varphi,\phi,t),\ \psi_\theta(\varphi,0,t) = \psi_\theta(\varphi,\phi,t) \end{aligned} \tag{17}$$

The physical compatibility conditions:

$$\begin{aligned} &N_\theta(\varphi,0,t) = N_\theta(\varphi,\phi,t),\ N_{\varphi\theta}(\varphi,0,t) = N_{\varphi\theta}(\varphi,\phi,t),\ Q_\theta(\varphi,0,t) = Q_\theta(\varphi,\phi,t) \\ &M_s(\varphi,0,t) = M_s(\varphi,\phi,t),\ M_{\varphi\theta}(\varphi,0,t) = M_{\varphi\theta}(\varphi,\phi,t) \end{aligned} \tag{18}$$

In order to satisfy the above requirements, the authors draw on the experience of two elastically coupled rectangular plates [56] to present a coupling spring technique which can be viewed as one innovation point of the present study. In this technique, three groups of linear and two groups of coupling springs are applied to imitate the kinematic compatibility and physical compatibility conditions of functionally graded parabolic and circular panels at the common meridian with $\theta = 0$ and 2π when consider a complete shell of revolution, as show in Fig. 2. Therefore, the potential energies (U_{cp}) stored in in the five types of coupling springs can be defined as:

$$U_{cp} = \frac{1}{2}\int_{-h/2}^{-h/2}\int_{\varphi 0}^{\varphi 1}\left\{\begin{array}{l} k_{uc}^{u}\left(u_0|_{\theta=0} - u_0|_{\phi=2\pi}\right)^2 + k_{vc}^{v}\left(v_0|_{\theta=0} - v_0|_{\phi=2\pi}\right)^2 \\ +k_{wc}^{w}\left(w_0|_{\theta=0} - w_0|_{\phi=2\pi}\right)^2 + K_{\varphi c}^{\varphi}\left(\psi_\varphi|_{\theta=0} - \psi_\varphi|_{\phi=2\pi}\right)^2 \\ +K_{\theta c}^{\theta}\left(\psi_\theta|_{\theta=0} - \psi_\theta|_{\phi=2\pi}\right)^2 \end{array}\right\} R_\varphi d\varphi dz \tag{19}$$

It should be noted that the stiffnesses of corresponding springs used at the common meridian with $\theta = 0$ and 2π of functionally graded parabolic and circular panels are revalued to be zero automatically.

2.3 Admissible displacement functions and Solution procedure

Recently, Li [24–26] proposed a modified Fourier series technique for Euler–Bernoulli beams with arbitrary boundary conditions. In this technique, each displacement of a beam is expressed as a standard cosine Fourier series with the addition of several supplementary terms which used to remove all the discontinuities potentially associated at the boundaries. The detailed theoretical analyses and mathematical principle can been seen in Refs [24–26]. In this paper, the modified Fourier series technique is further developed and extended to deal with the vibrations of composite laminated circular panels and shells of revolution with elastic boundary conditions. Therefore, each of the reference surface displacements or rotations of the normal of a shell can be written as a modified Fourier series as follows:

$$u_0(\varphi,\theta,t) = \left(\sum_{m=0}^{\infty}\sum_{n=0}^{\infty} A_{mn}^{u}\cos\lambda_m\varphi\cos\lambda_n\theta + \sum_{l=1}^{2}\chi_l(\theta)\sum_{m=0}^{\infty} a_m^l\cos\lambda_m\varphi + \sum_{l=1}^{2}\zeta_l(\varphi)\sum_{n=0}^{\infty} b_n^l\cos\lambda_n\theta\right)e^{j\omega t} \tag{20a}$$

$$v_0(\varphi,\theta,t) = \left(\sum_{m=0}^{\infty}\sum_{n=0}^{\infty} B_{mn}^{v}\cos\lambda_m\varphi\cos\lambda_n\theta + \sum_{l=1}^{2}\chi_l(\theta)\sum_{m=0}^{\infty} c_m^l\cos\lambda_m\varphi + \sum_{l=1}^{2}\zeta_l(\varphi)\sum_{n=0}^{\infty} d_n^l\cos\lambda_n\theta\right)e^{j\omega t} \tag{20b}$$

$$w_0(\varphi,\theta,t) = \left(\sum_{m=0}^{\infty}\sum_{n=0}^{\infty} C_{mn}^{w}\cos\lambda_m\varphi\cos\lambda_n\theta + \sum_{l=1}^{2}\chi_l(\theta)\sum_{m=0}^{\infty} e_m^l\cos\lambda_m\varphi + \sum_{l=1}^{2}\zeta_l(\varphi)\sum_{n=0}^{\infty} f_n^l\cos\lambda_n\theta\right)e^{j\omega t} \tag{20c}$$

$$\psi_\varphi(\varphi,\theta,t) = \left(\sum_{m=0}^{\infty}\sum_{n=0}^{\infty} D_{mn}^{\varphi}\cos\lambda_m\varphi\cos\lambda_n\theta + \sum_{l=1}^{2}\chi_l(\theta)\sum_{m=0}^{\infty} g_m^l\cos\lambda_m\varphi + \sum_{l=1}^{2}\zeta_l(\varphi)\sum_{n=0}^{\infty} h_n^l\cos\lambda_n\theta\right)e^{j\omega t} \tag{20d}$$

$$\psi_\theta(\varphi,\theta,t) = \left(\sum_{m=0}^{\infty}\sum_{n=0}^{\infty} E_{mn}^{\theta}\cos\lambda_m\varphi\cos\lambda_n\theta + \sum_{l=1}^{2}\chi_l(\theta)\sum_{m=0}^{\infty} k_m^l\cos\lambda_m\varphi + \sum_{l=1}^{2}\zeta_l(\varphi)\sum_{n=0}^{\infty} q_n^l\cos\lambda_n\theta\right)e^{j\omega t} \tag{20e}$$

where $\lambda_m = m\pi/\Delta\varphi$ (where $\Delta\varphi = \varphi_1 - \varphi_0$), $\lambda_n = n\pi/\phi$, and A^u_{mn}, B^v_{mn}, C^w_{mn}, D^φ_{mn}, D^θ_{mn} are the Fourier coefficients of two-dimensional Fourier series expansions for the displacements functions, respectively. a^l_m, b^l_n, c^l_m, d^l_n, e^l_m, f^l_n, g^l_m, h^l_n, k^l_m, q^l_n, are the supplemented coefficients of the auxiliary functions $\chi_l(\theta)$ and $\zeta_l(\varphi)$, where $l = 1, 2$. The two types of auxiliary functions $\chi_l(\theta)$ and $\zeta_l(\theta)$ are selected to remove all the discontinuities potentially associated with the first-order derivatives at the boundaries. Thus, the function sets are capable of representing any free vibration motion of the shell. The two types of auxiliary functions are given as:

$$\zeta(\varphi) = \begin{cases} \zeta_1(\varphi) = \frac{\Delta\varphi}{2\pi}\sin\left(\frac{\pi\overline{\varphi}}{2\Delta\varphi}\right) + \frac{\Delta\varphi}{2\pi}\sin\left(\frac{3\pi\overline{\varphi}}{2\Delta\varphi}\right) \\ \zeta_2(\varphi) = -\frac{\Delta\varphi}{2\pi}\cos\left(\frac{\pi\overline{\varphi}}{2\Delta\varphi}\right) + \frac{\Delta\varphi}{2\pi}\cos\left(\frac{3\pi\overline{\varphi}}{2\Delta\varphi}\right) \end{cases} \tag{21a}$$

$$\chi(\theta) = \begin{cases} \chi_1(\theta) = \frac{\phi}{2\pi}\sin\left(\frac{\pi\theta}{2\phi}\right) + \frac{\phi}{2\pi}\sin\left(\frac{3\pi\theta}{2\phi}\right) \\ \chi_2(\theta) = \frac{\phi}{2\pi}\cos\left(\frac{\pi\theta}{2\phi}\right) + \frac{\phi}{2\pi}\cos\left(\frac{3\pi\theta}{2\phi}\right) \end{cases} \tag{21b}$$

It is easy to verify that

$$\zeta_1(\varphi_0) = \zeta_1(\varphi_1) = \zeta_1'(\varphi_1) = 0,\ \zeta_1'(\varphi_0) = 1 \tag{22a}$$

$$\zeta_2(\varphi_0) = \zeta_2(\varphi_1) = \zeta_2'(\varphi_0) = 0,\ \zeta_2'(\varphi_1) = 1 \tag{22b}$$

$$\chi_1(0) = \chi_1(\phi) = \chi_1'(\phi) = 0,\ \chi_1'(0) = 1 \tag{22c}$$

$$\chi_2(0) = \chi_2(\phi) = \chi_2'(\phi) = 0,\ \chi_2'(\phi) = 1 \tag{22d}$$

The Lagrangian energy function (L) of the composite laminated circular panels and shells of revolution can be written as:

$$L = T - U_s - U_{sp} - U_{cp} \tag{23}$$

Substituting Eqs. (7)–(10), (16), (19) and (20) into Eq. (23). Then, the Lagrangian expression is minimized by taking its derivatives with respect to these coefficients:

$$\frac{\partial L}{\partial \chi} = 0,\ \chi = A^u_{mn}, a^l_m, b^l_n, B^v_{mn}, c^l_m, d^l_n, \cdots E^\theta_{mn}, g^l_m, h^l_n \tag{24}$$

Since the displacements and rotation components of the moderately thick functionally graded parabolic and circular panels and shells of revolution are chosen as $\mathbf{M}$ and $\mathbf{N}$ to obtain the results with acceptable accuracy, a total of $5 \times (\mathbf{M}+1) \times (\mathbf{N}+1) + 10 \times (\mathbf{M}+\mathbf{N}+2)$ equations are obtained. They can be summed up in a matrix form:

$$\left(\mathbf{K} - \omega^2\mathbf{M}\right)\mathbf{H} = \mathbf{0} \tag{25}$$

where $\mathbf{K}$, $\mathbf{M}$ and $\mathbf{H}$ respectively represent the stiffness matrix, mass matrix and vector of the unknown coefficients for the shell. The detail expressions for above matrices are given in Appendix B. By solving the Eq. (25), the frequencies (or eigenvalues) of composite laminated circular panels and shells of revolution can be readily obtained and the mode shapes can be yielded by substituting the corresponding eigenvectors into series representations of displacement and rotation components.

3 Results and discussions

In this section, the authors exhibit the vibration behaviors of moderately thick composite laminated circular panels and shells of revolution by means of the present method. Firstly, the convergence, accuracy and reliability of the present method are verified by the comparison with other methods. Secondly, based on the verification, some new results of moderately thick composite laminated circular panels and shells of revolution are presented. Lastly, the parameter study about the effects of the geometric and material parameters on the vibration behaviors of the circular panels and shells is reported. In addition, unless otherwise stated, the material properties used in following analyses are: $E_1 = 15E_2$, $E_2 = 10$ GPa, $G_{23} = 0.5E_2$; $G_{12} = G_{13} = 0.6E_2$, $\mu_{12} = 0.23$, $\rho = 1500\ \mathrm{kg/m^3}$.

3.1 Convergence study

From the theoretical formulations, we can know that the computational accuracy relies on a limited number of terms in the displacement expressions in actual calculation. Thus, it is very important to check its convergence. In order to simplify this study, a symbolism is employed to represent the boundary condition of a composite laminated circular panels and shells of revolution, *e.g.* the FCSE and CF respectively denote the panels with F (Free), C (Clamped), S (simply-support) and E (Elastic restrain) boundary conditions at $\varphi = \varphi_0$, $\theta = 0$, $\varphi = \varphi_1$ and $\theta = \phi$ and the shells with C (Clamped) and F (Free) at $\varphi = \varphi_0$ and $\varphi = \varphi_1$. The convergence of the first eight frequency parameters for composite laminated circular toroid and Toro-circular panel with complete clamped boundary conditions is presented in Table 2. The geometrical parameters and layout for the composite laminated circular toroid and Toro-circular panel used in the study are: Toro-circular panel: $R_b = -1.5$ m and 1.5 m, $R = 3$ m, $h = 0.2$ m, $\varphi_0 = 60^\circ$, $\varphi_1 = 120^\circ$, $\phi = 120^\circ$, $[0^\circ/90^\circ/0^\circ]$; Circular

Table 2: Convergence of frequency parameters Ω for clamped composite laminated Toro-circular panel and circular toroid with different truncation terms M and N.

Shape	R_b	$M \times N$	Mode number							
			1	2	3	4	5	6	7	8
Circular toroid with [0°/90°]	−1.5	10×10	2.2596	2.2596	2.4146	2.4146	2.6191	2.6191	2.8426	2.8426
		11×11	2.2596	2.2596	2.4146	2.4146	2.6191	2.6191	2.8426	2.8426
		12×12	2.2596	2.2596	2.4146	2.4146	2.6191	2.6191	2.8426	2.8426
		13×13	2.2596	2.2596	2.4146	2.4146	2.6191	2.6191	2.8426	2.8426
		14×14	2.2596	2.2596	2.4146	2.4146	2.6191	2.6191	2.8426	2.8426
	1.5	10×10	2.1568	2.1568	2.1631	2.1631	2.2010	2.2010	2.2264	2.2264
		11×11	2.1568	2.1568	2.1631	2.1631	2.1947	2.1947	2.2264	2.2264
		12×12	2.1568	2.1570	2.1631	2.1631	2.1944	2.1944	2.2264	2.2264
		13×13	2.1568	2.1568	2.1631	2.1631	2.1943	2.1943	2.2264	2.2264
		14×14	2.1568	2.1568	2.1631	2.1631	2.1943	2.1943	2.2264	2.2264
Toro-circular panel with [0°/90°/0°]	−1.5	10×10	3.0041	3.5867	3.7325	4.0905	4.6909	5.0980	5.1652	5.4625
		11×11	3.0041	3.5867	3.7324	4.0905	4.6909	5.0980	5.1652	5.4625
		12×12	3.0041	3.5866	3.7324	4.0905	4.6909	5.0980	5.1652	5.4625
		13×13	3.0041	3.5866	3.7324	4.0905	4.6909	5.0980	5.1652	5.4625
		14×14	3.0040	3.5866	3.7324	4.0905	4.6909	5.0980	5.1652	5.4625
	1.5	10×10	2.6711	2.8511	2.9112	2.9297	2.9315	2.9787	2.9958	3.0342
		11×11	2.6711	2.8511	2.9112	2.9297	2.9315	2.9787	2.9958	3.0342
		12×12	2.6711	2.8511	2.9112	2.9297	2.9315	2.9787	2.9958	3.0342
		13×13	2.6711	2.8511	2.9112	2.9297	2.9315	2.9787	2.9958	3.0342
		14×14	2.6711	2.8511	2.9112	2.9297	2.9315	2.9787	2.9958	3.0342

toroid: $R_b = -1.5$ m and 1.5 m, $R = 3$ m, $h = 0.2$ m, $\varphi_0 = 60°$, $\varphi_1 = 120°$, $\phi = 360°$, [0°/90°]. Five groups of truncation terms are performed in the examination, *i.e.* $M = N = 10$, 11, 12, 13 and 14. It is evident that the present method has an excellent convergence, and is sufficiently accurate even when only a small number of terms are included in the series expressions. Taking both the computational accuracy and efficiency into consideration, in following examples, the truncated number of the displacement expressions will be uniformly selected as $M \times N = 12 \times 12$. Furthermore, in order to validate the accuracy and reliability of current solution, more numerical examples will be presented. In each case, the convergence study is performed and for brevity purposes, only the converged results are presented here.

3.2 Validation and new results

As mentioned earlier, the complete shells can be obtained by means of three groups of linear coupling springs and two groups of rotational coupling springs to imitate the kinematic compatibility and physical compatibility conditions at the coupling boundary condition when the circumference angle of the panels is equal to 2π. Thus, before the validation of the present method, the influence of the stiffnesses of coupling spring on vibration behavior of the panels should be investigated first. Table 3 shows the first four frequency parameter $\Omega = \omega R\sqrt{\rho/E_2}$ for composite laminated Toro-circular panel with different coupling springs. The all types of coupling springs, *i.e.* $k_{uc} = k_{vc} = k_{wc} = K_{\varphi c} = K_{\theta c}$, uniformly vary from $10^0 D$ to $10^8 D$, where $D = E_1 h^3/12\left(1-\mu^2\right)$. According to the Table 3, we can see that the frequency parameter monotonously increases with the increasing of the values of the stiffness of coupling springs. Furthermore, the mechanical behavior of the panels gradually approaches a complete shell, and lastly remain unchanged while the stiffnesses of coupling spring reach the infinity. So, the values of the stiffness of coupling springs will be uniformly selected as $k_{uc} = k_{vc} = k_{wc} = K_{\varphi c} = K_{\theta c} = 10^6 D$.

Next, the validation work for circular panels and shells of revolution with classical boundary conditions will be performed by using the present method. Table 4 shows the frequency parameters Ω for a three-layered, symmetrical cross-ply [0°/90°/0°] spherical dome with different classical boundary conditions. The first ten circumferential wave number, *i.e.* $n = 0 - 9$, are consid-

ered in the comparison. The geometric and material constants of the spherical shell are: E_1 = 138 GPa, E_2 = 10.6 GPa, G_{12} = 6 GPa; G_{13} = G_{23} = 3.9 GPa, μ_{12} = 0.28, ρ = 1500 kg/m^3, R = 1 m, h = 0.05 m, R_b = 0 m, φ_0 = 60°, φ_1 = 90°. The results provided by Ye *et al.* [1] and Qu *et al.* [4] based on a FSDT formulation are selected as the benchmark solutions. Table 5 shows frequency parameters Ω for a four-layer, unsymmetrical cross-ply [0°/90°/0°/90°] spherical dome with five groups of classical boundary conditions. The geometric parameters of the spherical dome are: R = 1 m, h = 0.1 m, R_b = 0 m and φ_0 = 15°, 30° and 45°, φ_1 = 90°. The reference results are given by Ye *et al.* [1] *et al.* based on the FSDT formulation. The comparison of the frequency parameters Ω for a four-layered, unsymmetrical cross-ply [45°/−45°/45°/−45°] spherical panels with different classical boundary conditions obtained from the present method and other theories and methods [3, 11] is shown in Table 6. The panels parameters used in the comparison are as follows: E_1 = 150 GPa, E_2 = 10 GPa, G_{12} = 6 GPa; G_{12} = G_{13} = G_{23} = 0.5E_2, μ_{12} = 0.23, ρ = 1700 kg/m^3, R = 10 m, h = 0.01 m, R_b = 0 m, φ_0 = 87.1°, φ_1 = 92.9°, ϕ = 11.5°. Also, the validity of the present method for three-layered, symmetrical composite laminated spherical panels with different classical boundary conditions is shown in Table 7. The geometric and material constants of the spherical panels are: E_1 = 60.7 GPa, E_2 = 24.8 GPa, G_{12} = G_{13} = G_{23} = 12 GPa, μ_{12} = 0.23, ρ = 1700 kg/m^3, R = 2 m, h = 0.05 m, R_b = 0 m, φ_0 = 75.5°, φ_1 = 104.5°, ϕ = 28.6°. Four sets of lamination schemes, *i.e.*, [0°/0°/0°], [15°/−15°/15°], [30°/−30°/30°] and [45°/−45°/45°], are performed in the comparison. For comparison, the reference results given by Ye *et al.* [2, 3] based on CST and FSDT are also listed in the table. Lastly, Table 8 shows the comparison work of the first ten frequencies (Hz) for an isotropic Toro-circular panel with the CFCF boundary and circular toroid with the SS boundary condition. The geometric and material constants of the Toro-parabolic panel and Circular toroid are: Toro-parabolic panel: Toro-circular panel: R_b = −1.5 m, R = 3 m, h = 0.2 m, φ_0 = 60°, φ_1 = 120°, ϕ = 120°, E = 168 GPa, μ = 0.3, ρ = 5700 kg/m^3; Circular toroid: R_b = −1.5 m, R = 3 m, h = 0.2 m, φ_0 = 60°, φ_1 = 120°, ϕ = 360°, E = 168 GPa, μ = 0.3, ρ = 5700 kg/m^3. The reference results given by Tornabene *et al.* [53] using the GDQ method on the basis of FSDT are used to verify the accuracy of the proposed method. From the Tables 4–8, we can see a consistent agreement of present results and referential data.

Through the above analyses, the good accuracy and convergence of the present method can be validated, which enhances the confidence that it can be used to predicate the vibration behaviors of composite laminated circular panels and shells of revolution with elastic boundary conditions. Tables 9–10 show the lowest five frequency parameters Ω for composite laminated circular toroid with various boundary conditions including classical and elastic boundary conditions. New vibration results of the composite laminated Toro-circular panels are given in Tables 11–12. The geometric constants of the circular toroid and the Toro-circular panel are the same as Table 8. Three sets of lamination schemes, *i.e.*, [0°/90°], [0°/90°/0°] and [0°/90°/0°/90°], are performed in the above analysis. Those results can be served as benchmark results for the future computational methods in this filed. From the Tables, we can see that the vibration characteristics of the composite laminated circular panels and shells of revolution strongly depend on the boundary condition and material parameters. As mentioned before, the mode shapes of the composite laminated circular panels and shells of revolution can be obtained by substituting the corresponding eigenvectors into series representations of displacement and rotation components. So, for illustrative purposes, some selected mode shapes of the aforementioned structures are depicted in Figs. 3–4. From these figures, the vibration behaviors of the panels and shells subjected to different boundary conditions can be seen vividly, which can enhance our understanding of the vibration characteristics of composite laminated circular panels and shells of revolution.

3.3 Some parameters study

As is well known, the fiber orientation angle, boundary restrain parameters, layer number, circumferential angle and stiffness ratio have a significant impact on the vibration behavior of the structures. Fig. 5 shows the variation of the frequency parameters Ω for a moderately thick composite laminated circular toroid with different boundary restrain parameters Γ_λ. The variation for a moderately thick composite laminated Toro-circular panel with different boundary restrain parameters Γ_λ are shown in Fig. 6. The geometrical parameters of the circular toroid and Toro-circular panel are the same as the Tables 9–12. From the Figs. 5–6, we can know that the frequency parameters Ω increases with the increasing of the boundary restrain parameters irrespective of the types of boundary springs. In addition, it is obvious that the vibration behavior of above structures almost doesn't change while the Γ_λ is less than $10^{-2}D$, then the change of vibration behavior is very intensity when the Γ_λ is under the certain range of $[10^{-2}D, 10^6D]$, and lastly remains unchanged when the Γ_λ

Table 3: Effect of stiffnesses of coupling spring on frequency parameters Ω for Toro-circular panel.

$k_{uc} = k_{vc} = k_{wc} =$	$R_b = -1.5$				$R_b = 1.5$			
$K_{\varphi c} = K_{\theta c}$	1	2	3	4	1	2	3	4
10^0D	2.0577	2.0764	2.2084	2.2660	1.8485	2.0458	2.1588	2.1601
10^1D	2.2016	2.2274	2.3646	2.3942	1.9066	2.1305	2.1588	2.1604
10^2D	2.2438	2.2460	2.4062	2.4065	2.0886	2.1525	2.1590	2.1614
10^3D	2.2574	2.2575	2.4132	2.4134	2.1542	2.1563	2.1610	2.1627
10^4D	2.2594	2.2594	2.4144	2.4145	2.1566	2.1567	2.1628	2.1630
10^5D	2.2596	2.2596	2.4146	2.4146	2.1568	2.1568	2.1631	2.1631
10^6D	2.2596	2.2596	2.4146	2.4146	2.1568	2.1568	2.1631	2.1631
10^7D	2.2596	2.2596	2.4146	2.4146	2.1568	2.1568	2.1631	2.1631
10^8D	2.2596	2.2596	2.4146	2.4146	2.1568	2.1568	2.1631	2.1631

Table 4: Comparison of the frequency parameters Ω for a three-layered, cross-ply [0°/90°/0°] spherical dome with different restraints.

n	Ref [4]			Ref [1]			Present		
	SDSD	SS	CC	SDSD	SS	CC	SDSD	SS	CC
0	0.50303	3.89549	4.33683	0.50295	3.89403	4.33555	0.50303	3.89584	4.33714
1	0.91228	3.58229	3.9707	0.91165	3.58099	3.96964	0.91237	3.58262	3.97097
2	1.60951	3.37675	3.82405	1.60828	3.3754	3.82291	1.60973	3.37710	3.82435
3	2.12446	3.29465	3.77315	2.12345	3.29326	3.77197	2.12798	3.29501	3.77345
4	2.12385	3.27189	3.76161	2.12275	3.2705	3.76042	2.13065	3.27226	3.76192
5	2.16404	3.28458	3.77361	2.16293	3.28319	3.77242	2.16436	3.28494	3.77392
6	2.25058	3.32575	3.80616	2.24946	3.3244	3.80499	2.25428	3.32609	3.80648
7	2.37899	3.39491	3.86069	2.37788	3.39359	3.85954	2.37985	3.39520	3.86108
8	2.54685	3.49381	3.94014	2.54574	3.49255	3.93902	2.55656	3.49429	3.94107
9	2.75233	3.62469	4.0477	2.75123	3.62349	4.04663	2.76281	3.62578	4.05149

Table 5: Comparison of the frequency parameters Ω for a four-layered, cross-ply [0°/90°/0°/90°] spherical dome with different restraints.

φ_0	Mode	Ref [1]					present				
		FF	SDSD	SS	SC	CC	FF	SDSD	SS	SC	CC
15°	1	0.24139	0.63549	1.93103	2.02086	2.02830	0.24148	0.63554	1.93189	2.02196	2.02933
	2	0.61925	0.93741	2.00323	2.18373	2.18409	0.61938	0.94280	2.00316	2.18423	2.18454
	3	1.09809	1.35136	2.19406	2.39252	2.39428	1.09811	1.35312	2.19381	2.39283	2.39452
	4	1.15710	1.49074	2.37353	2.41032	2.54640	1.15682	1.49198	2.37379	2.41006	2.54624
	5	1.47910	1.68819	2.37813	2.43522	2.57792	1.47887	1.68978	2.37806	2.43500	2.57782
30°	1	0.23228	0.75173	2.25763	2.34867	2.43409	0.23270	0.75181	2.25857	2.34971	2.43524
	2	0.61199	1.04009	2.31336	2.45545	2.56885	0.61276	1.04344	2.31434	2.45657	2.56994
	3	0.61430	1.42146	2.42157	2.59831	2.69277	0.61483	1.42475	2.42231	2.59937	2.69368
	4	1.09612	1.65300	2.64933	2.86301	2.92038	1.09692	1.65714	2.64971	2.86392	2.92109
	5	1.43748	1.71311	2.78325	2.96718	3.15755	1.43641	1.71347	2.78231	2.96640	3.15709
45°	1	0.21980	0.76685	2.53619	2.79107	3.03174	0.21984	0.76683	2.53671	2.79181	3.03273
	2	0.37627	1.07386	2.58002	2.83598	3.07735	0.37622	1.07569	2.58056	2.83653	3.07849
	3	0.59911	1.67145	2.65484	2.85380	3.14996	0.59917	1.67625	2.65506	2.85453	3.15112
	4	0.98701	1.8397	2.76414	3.03830	3.30904	0.98680	1.84808	2.76455	3.03894	3.31016
	5	1.08266	1.93303	3.08872	3.35597	3.58253	1.08276	1.93385	3.08960	3.35716	3.58413

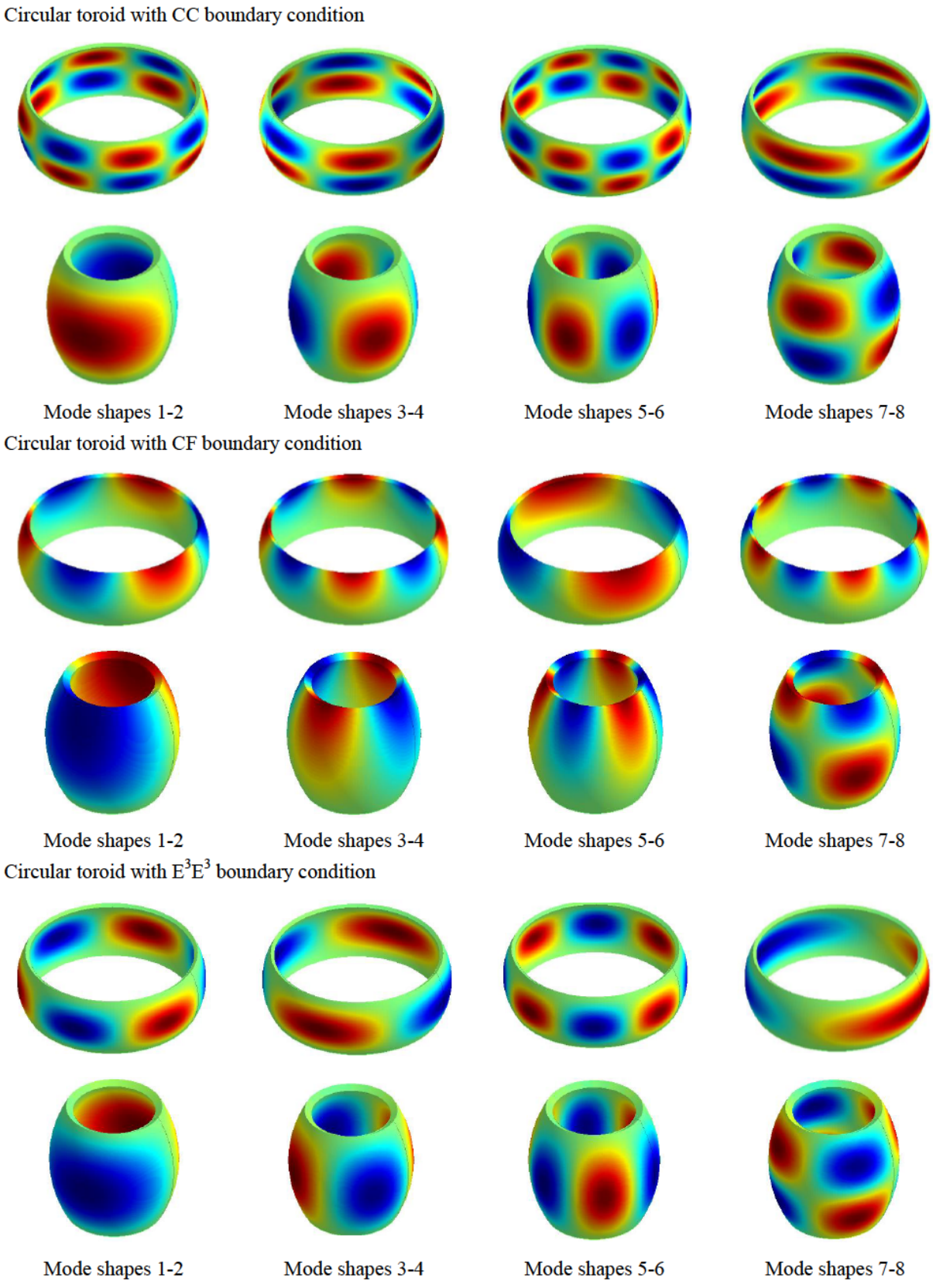

Figure 3: Mode shapes of the circular toroid with different boundary conditions.

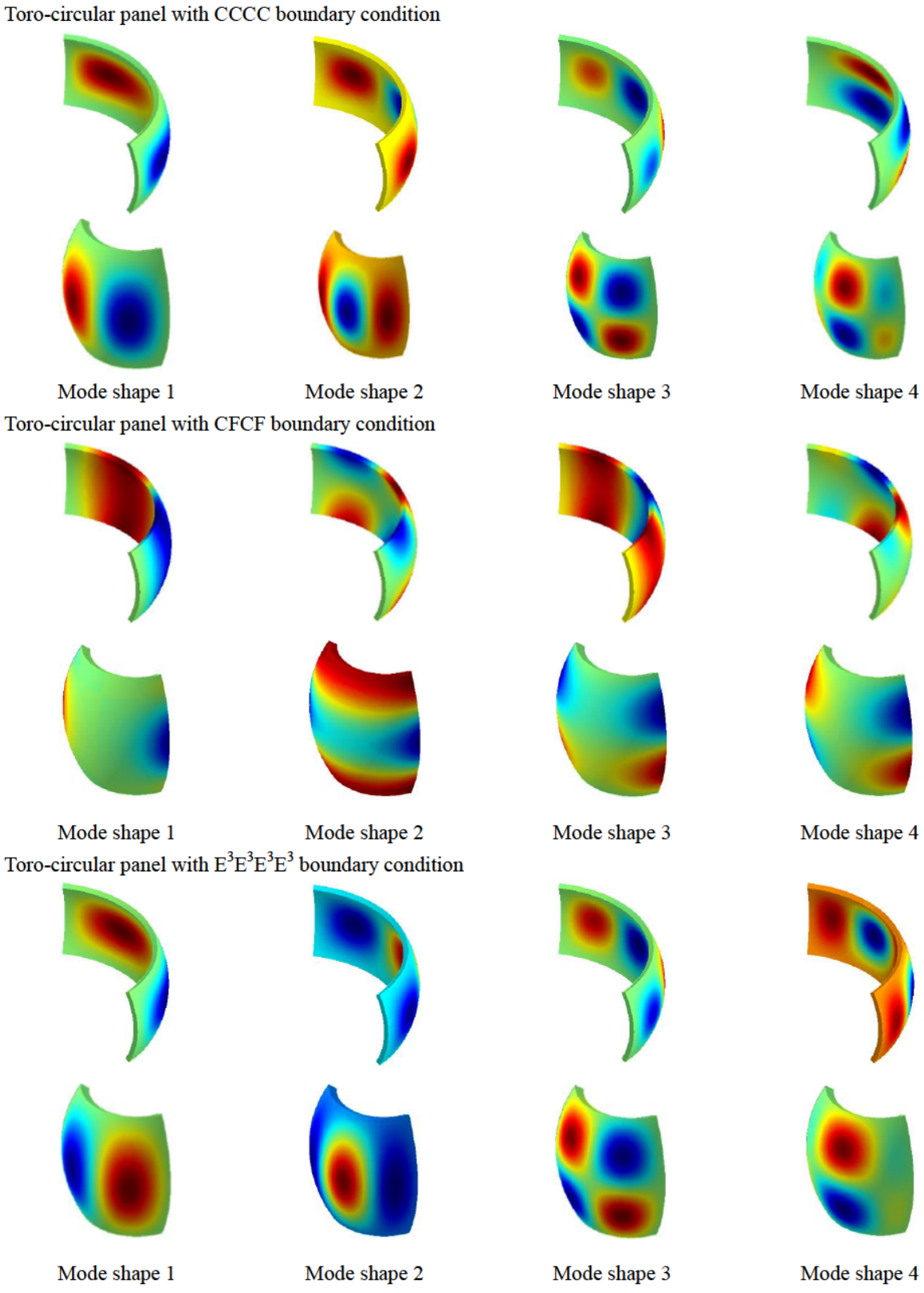

Figure 4: Mode shapes of the Toro-circular panel with different boundary conditions.

Table 6: Comparison of the frequency parameters Ω for a four-layered, cross-ply [45°/−45°/45°/−45°] spherical panels with different restraints.

Method	Mode	Boundary condition							
		FFFF	FSFS	FFFC	FCFC	FCCC	SSSS	SCSC	CCCC
Ref [3]	1	2.3732	7.6886	0.5360	10.119	12.550	31.799	32.310	35.898
	2	5.8131	10.895	3.0887	11.429	15.220	34.178	34.599	36.700
	3	8.2261	13.397	3.1118	13.425	22.351	34.947	35.113	40.645
	4	12.141	16.703	9.0389	17.729	26.440	37.594	38.487	42.597
	5	14.152	17.83	9.4796	20.388	32.857	42.428	44.898	48.469
	6	19.369	22.328	16.037	24.034	35.394	43.625	45.858	52.539
Ref [11]	1	2.3712	7.6402	0.5347	10.033	12.529	31.727	32.229	35.827
	2	5.7853	10.856	3.0688	11.402	15.125	34.127	34.542	36.612
	3	8.1646	13.378	3.0946	13.403	22.147	34.884	35.043	40.488
	4	12.072	16.629	8.9686	17.61	26.335	37.521	38.394	42.361
	5	14.063	17.751	9.4149	20.221	32.519	42.303	44.741	48.183
	6	19.224	22.161	15.910	23.911	35.215	43.500	45.668	52.218
Present	1	2.3711	7.6729	0.5514	9.9574	12.526	31.728	32.230	35.828
	2	5.7857	10.971	3.0626	11.423	15.108	34.127	34.542	36.612
	3	8.1633	13.249	3.2994	13.390	22.153	34.884	35.043	40.489
	4	12.073	16.212	8.9849	17.941	26.330	37.521	38.395	42.362
	5	14.062	17.894	9.3614	20.188	32.535	42.302	44.745	48.183
	6	19.220	22.491	15.898	23.978	35.181	43.500	45.664	52.222

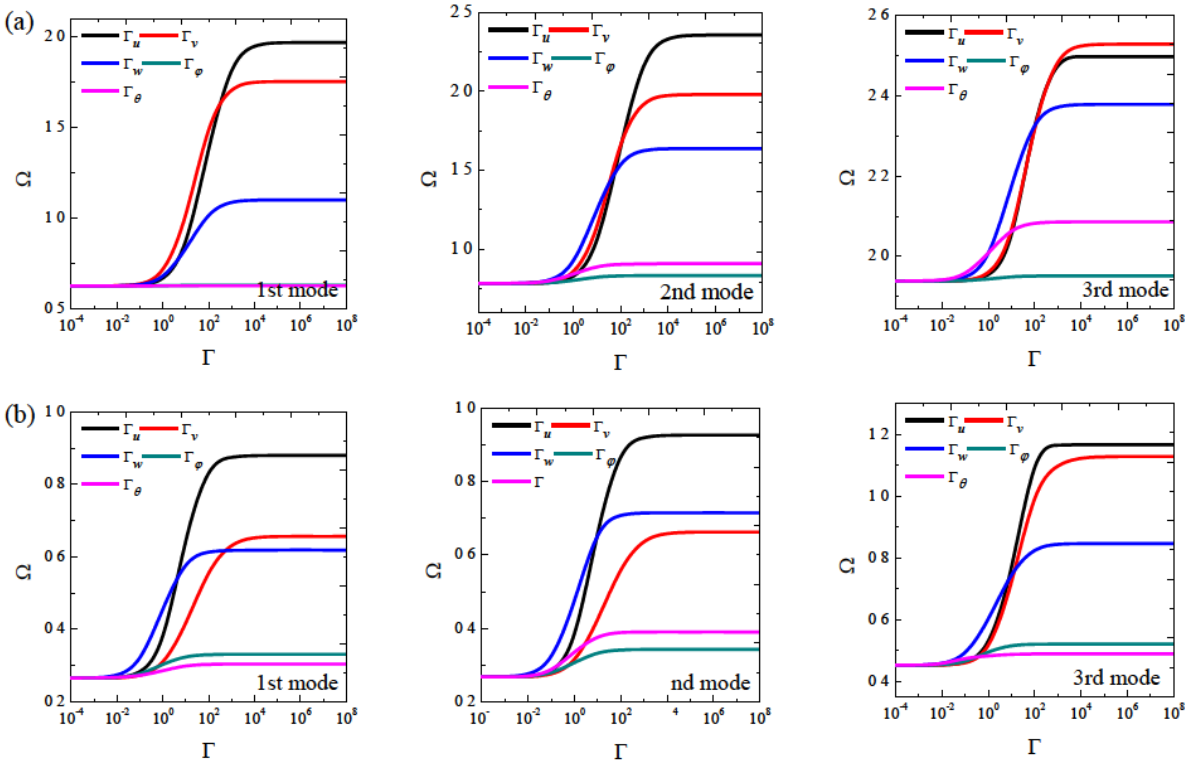

Figure 5: Frequencies of an moderately thick composite laminated circular toroid with Γ_λ elastic boundary conditions:(a) [0°/90°/0°/90°] and $R_b = -1.5$; (b) [0°/90°/0°] and $R_b = 1.5$.

Table 7: Comparison of the frequency parameters Ω for a certain three-layered spherical panels with different restraints.

Layout	Method	Mode number								
		1	2	3	4	5	6	7	8	9
[0°/0°/0°]	Ref [2]	8.14234	12.3699	13.9511	18.1169	20.0452	25.8037	26.2185	27.4026	28.2361
	Ref [3]	8.15995	12.4546	14.0268	18.3345	20.1208	26.0524	-	-	-
	Present	8.18682	12.4855	14.0546	18.4232	20.1964	26.2568	26.3334	27.4031	28.2366
[15°/−15°/15°]	Ref [2]	8.46704	12.6346	13.906	18.3054	20.4441	25.6776	26.1499	29.2057	29.9994
	Ref [3]	8.49083	12.7503	14.0083	18.5618	20.5703	25.8244	-	-	-
	Present	8.51746	12.7632	14.0326	18.6420	20.6301	25.8206	26.6430	29.2065	30.1342
[30°/−30°/30°]	Ref [2]	9.09300	12.9552	13.847	18.662	21.3978	24.3233	26.6959	30.0401	32.5608
	Ref [3]	9.14088	13.1156	14.0273	18.9934	21.6139	24.5616	-	-	-
	Present	9.15363	13.1043	14.0392	19.0534	21.6479	24.5417	27.2483	30.6758	32.5618
[45°/−45°/45°]	Ref [2]	9.39614	12.9945	13.8463	18.8344	22.4252	23.0589	26.8818	30.1109	34.1877
	Ref [3]	9.48125	13.1635	14.0772	19.2011	22.6695	23.3465	-	-	-
	Present	9.39089	13.1527	14.0804	19.1993	22.6671	23.0884	27.4516	30.7997	34.1908

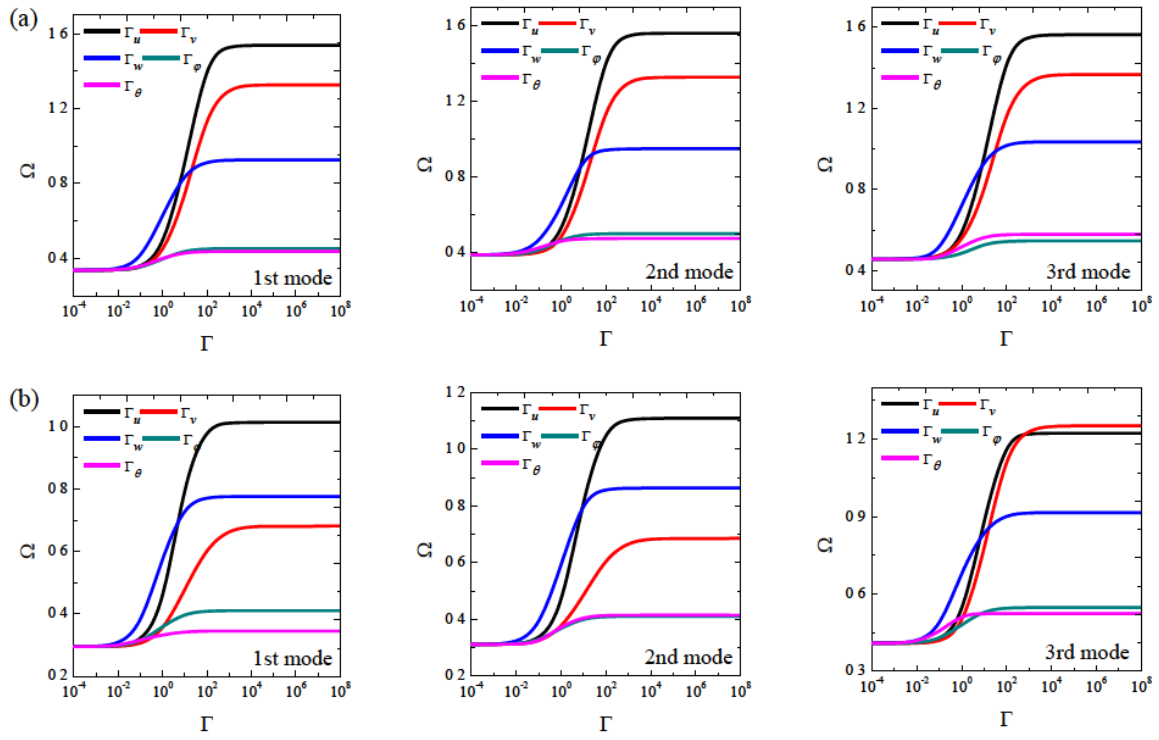

Figure 6: Frequencies of an CFCF moderately thick composite laminated Toro-circular panel with Γ_λ elastic boundary conditions:(a) [0°/90°/0°/90°] and R_b=-1.5; (b) [0°/90°/0°] and $R_b = 1.5$.

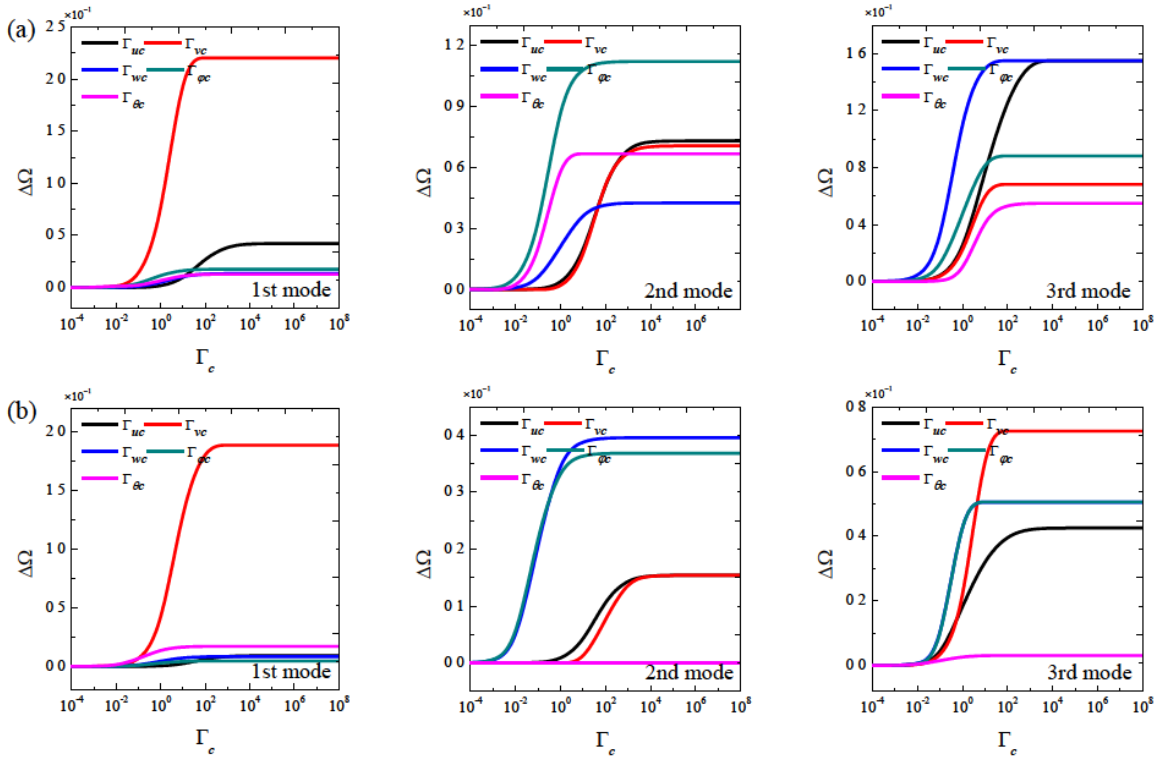

Figure 7: Frequencies of an moderately thick composite laminated Toro-circular panel with Γ_c elastic coupling conditions:(a) [0°/90°/0°/90°] and $R_b = 1.5$; (b) [0°/90°/0°] and $R_b = -1.5$.

Table 8: Comparison of the first ten frequencies (Hz) for an isotropic Toro-circular panel with CFCF boundary condition and circular toroid with SS boundary condition.

Mode	Circular toroid			Toro-circular panel		
	Ref [52]	Present	Error(%)	Ref [52]	present	Error(%)
1	342.58	342.21	0.11	251.74	252.18	0.18
2	342.58	342.21	0.11	255.73	256.18	0.17
3	374.73	374.82	0.02	338.95	339.14	0.06
4	374.73	374.82	0.03	347.75	348.02	0.08
5	377.88	377.30	0.15	363.74	363.05	0.19
6	377.88	377.30	0.15	409.79	410.46	0.16
7	438.80	439.97	0.27	472.68	471.76	0.20
8	481.90	481.12	0.16	562.05	561.37	0.12
9	481.91	481.12	0.16	627.51	627.88	0.06
10	485.20	484.79	0.08	628.42	628.79	0.06

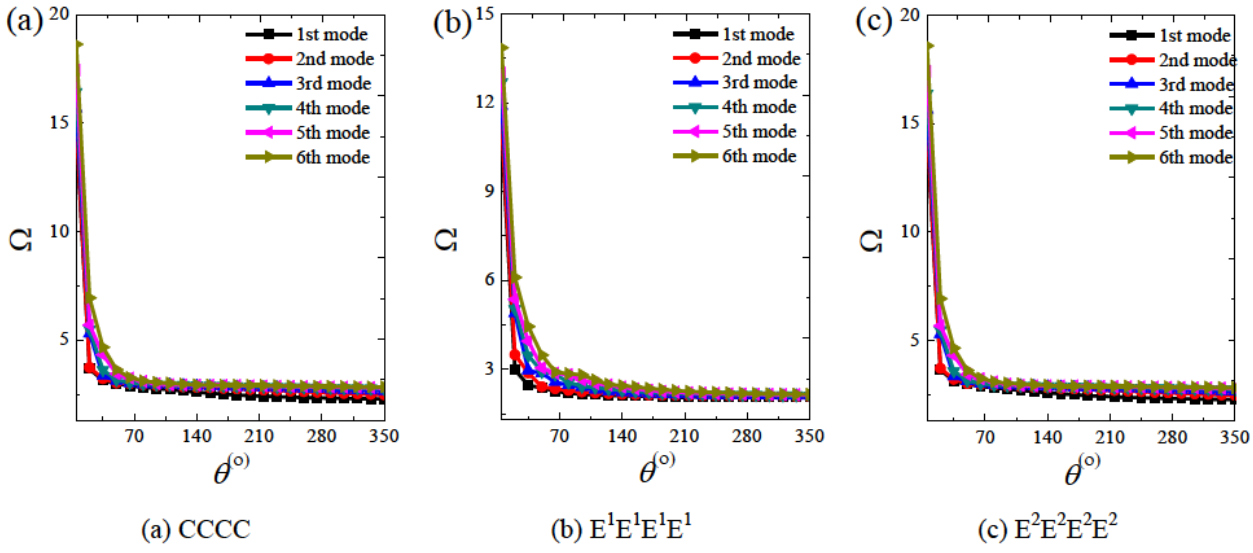

Figure 8: Frequencies of a [0°/90°/0°] Toro-circular panel with different circumference angles: (a) CCCC; (b) $E^1E^1E^1E^1$; (c) $E^2E^2E^2E^2$.

approaches infinity. Fig. 7 shows the influence of the coupling restrain parameters Γ_λ on the vibration behavior of Toro-circular panels. From the figure, it can be seen that for different types of coupling springs, this extent of the frequency parameter Ω is different. Next, the effect of the circumference angle on the vibration behavior of composite laminated Toro-circular panels will be revealed, and the variation of the first six frequency parameters Ω of the composite laminated Toro-circular panel with different boundary conditions and circumference angles is presented in Fig. 8. It is evident that the frequency parameters Ω monotonously decrease while the circumference angle increases. Next, the focus turns to the material itself attributes. Fig. 9 and Fig. 10 respectively indicate the variations of the lowest five frequency parameters Ω versus the stiffness ratio E_1/E_2 increasing from 1 to 100. From the figures, we can know that the frequency parameters Ω monotonously increase as the stiffness ratio increases regardless of the structure shapes and boundary conditions. It should be noted that the scope of influence of frequency parameters decreases in the same interval region of the stiffness ratio with the stiffness ratio E_1/E_2 increasing. Fig. 11 and Fig. 12 show the influence of the number of layers on the frequency parameters Ω of the $(0°/90°)_n$ composite laminated circular toroid and Toro-circular panel with different boundary conditions. As clearly observed from Figs. 11–12, the frequency parameters of the structures increase rapidly and may reach their crest around $n = 6$ (12 layer), and beyond this range, the frequency parameters remain unchanged. In such a case, the struc-

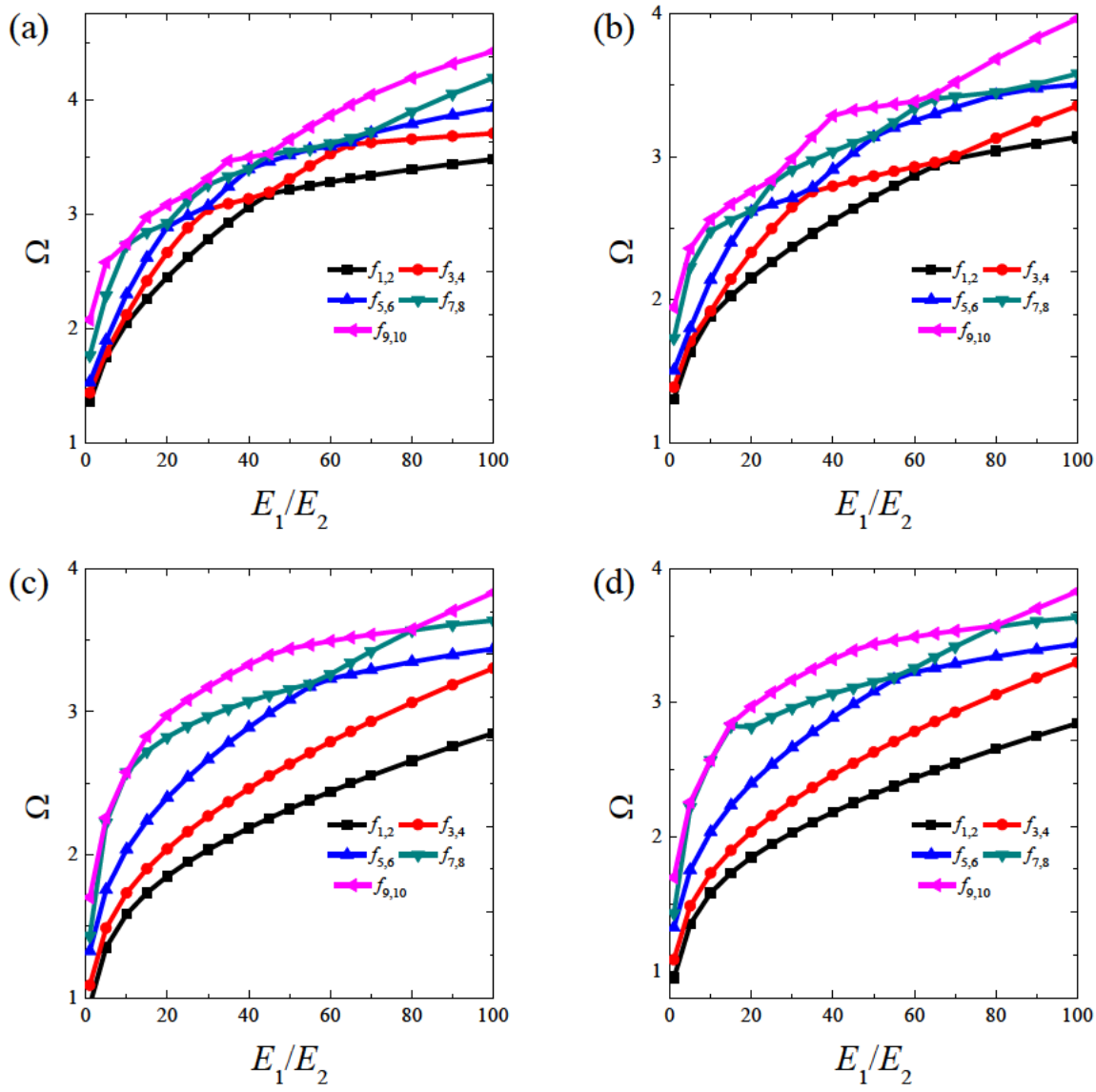

Figure 9: Frequencies of a [0°/90°] circular toroid ($R_b = -1.5$) with different stiffness ratios E_1/E_2: (a) CC; (b) SS; (c) E^1E^1; (d) E^3E^3.

tures can be treated as an orthotropic structure. As the last case of this sub-section, the influence of the fiber orientations α on the lowest six mode frequency parameters of the composite laminated circular toroid and Toro-circular panel is investigated. In Figs. 13 and 14, the variations of the lowest six frequency parameters Ω of the composite laminated circular toroid and Toro-circular panel with the CF and CFCF boundary condition against the fiber orientations α are depicted, respectively. Four laminated schedules, *i.e.* [0°/α°], [α°/0°], [0°/α°/0°] and [α°/0°/α°], are used in the examination. The geometrical parameters of the circular toroid and Toro-circular panel are the same as the Tables 9–12. From the figures, we can see that the fiber orientation α is a crucial factor to determine the vibration behavior of the composite laminated circular toroid and Toro-circular. Besides, many interested characteristics can be observed from the figures. Firstly, all the figures are symmetrical about $\alpha = 90°$; Secondly, there exists obvious differences between the frequency traces of the shell with [0°/α°] lamination and those of [α°/0°].

Through the above studies, we can know that the present method can be universally applied to composite laminated circular panels and shells of revolution with general boundary conditions including classical cases, elastic restraints and their combinations. Compared with the existing methods, the present method doesn't need any change to the solution procedure when the boundary conditions change. Besides, the boundary condition, geometric and the material parameters have a significant im-

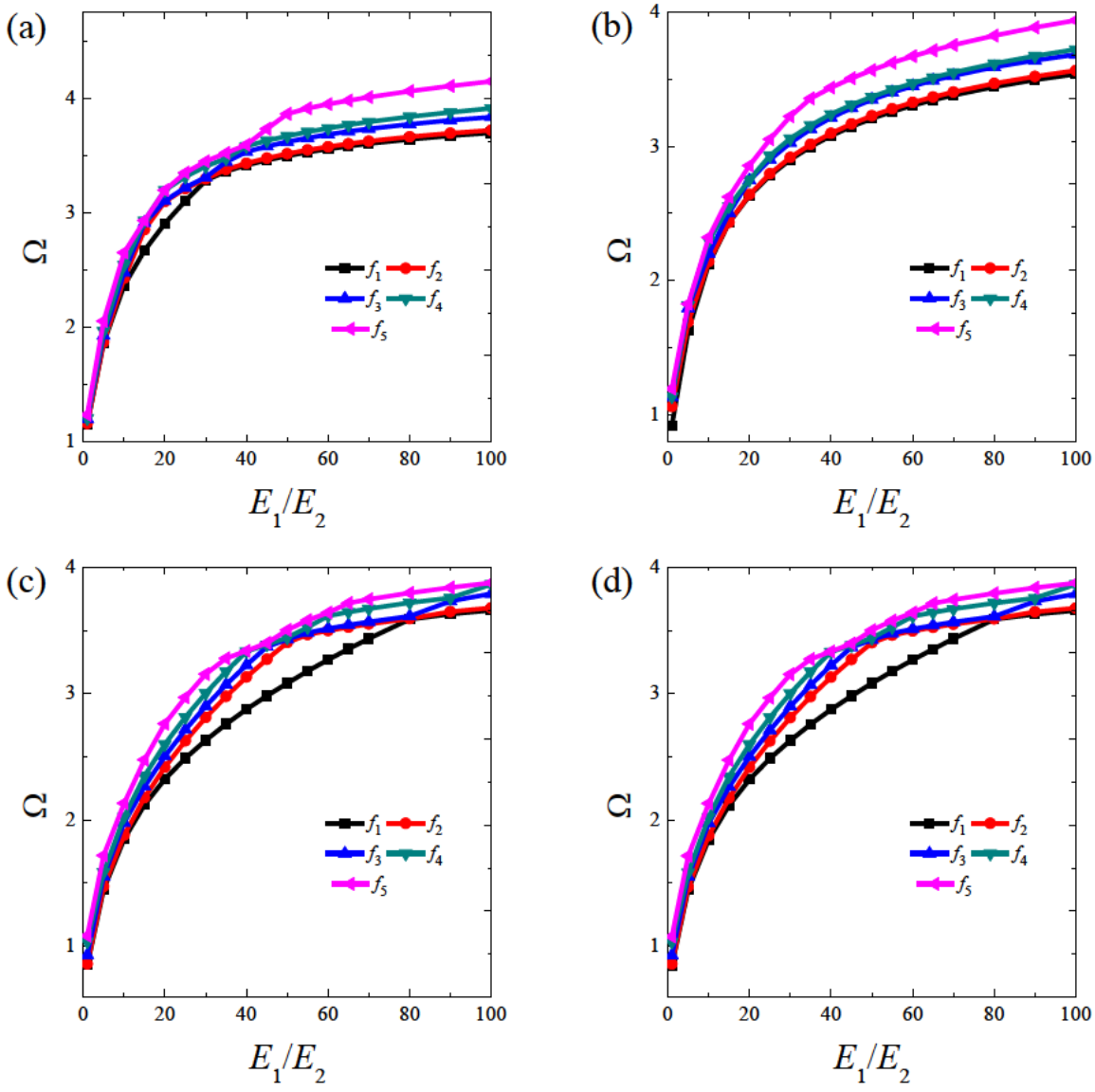

Figure 10: Frequencies of a [0°/90°/0°] Toro-circular panel ($R_b = 1.5$) with different stiffness ratios E_1/E_2: (a) CCCC; (b) SSSS; (c) $E^1E^1E^1E^1$; (d) $E^3E^3E^3E^3$.

pact on the vibration characteristics of the composite laminated circular panels and shells of revolution.

4 Conclusions

A unified method is presented for predicting the linear vibration of the composite laminated circular panels and shells of revolution with arbitrary boundary conditions. The approach employs the first-order shear deformation plate theory which includes the effects of rotary inertias and shear deformation. The admissible function of the composite laminated circular panels and shells of revolution is obtained by the improved Fourier series which consists of a superposition of the standard cosine Fourier series and several auxiliary functions introduced to remove any potential discontinuous of the original displacement and its derivatives at the boundaries. The arbitrary boundary condition can be achieved by the boundary spring technique in which three types of liner and two types of rotation springs along the edges of the circular panels and shells of revolution are adopted. In addition, the complete shells of revolution can be achieved by using the coupling spring technique to imitate the kinematic compatibility and physical compatibility conditions of composite laminated circular panels at the common meridian with

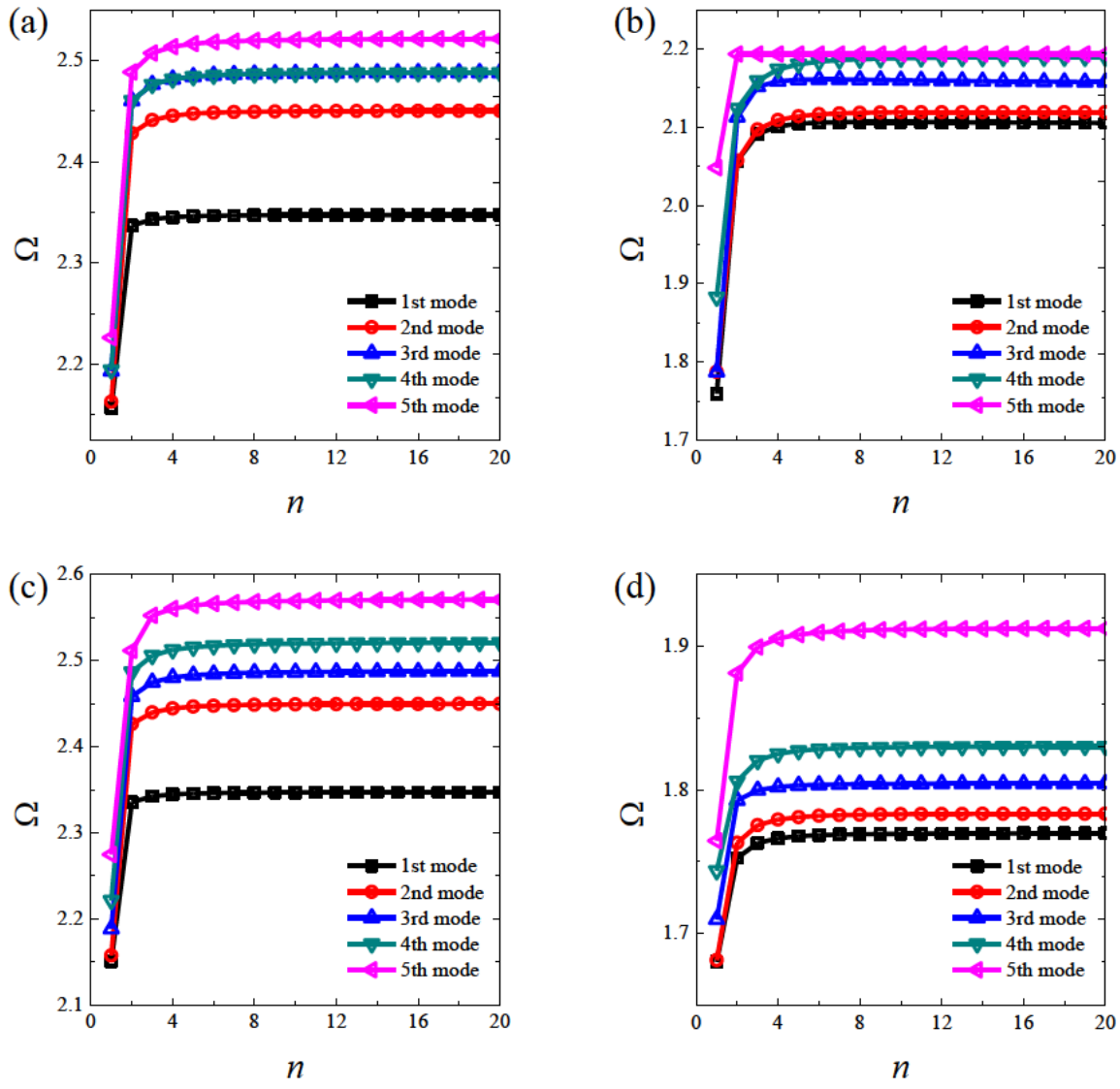

Figure 11: Frequencies of a $[0/90^\circ]_n$ circular toroid ($R_b = 1.5$) with different boundary conditions: (a) CC; (b) SS; (c) E^2E^2; (d) E^3E^3.

$\theta = 0$ and 2π. The convergence, accuracy and reliability of the present solutions are validated by numerical examples and the comparison between the present results and those available in the literature. In addition, the influence of boundary and coupling restraint parameters, circumference angles, stiffness ratios, numbers of layer and fiber orientations on the vibration behavior of the composite laminated circular panels and shells of revolution is also presented. Numerous new free vibration results for the composite laminated circular panels and shells of revolution with different lamination schemes and elastic restraints are presented. The following conclusions can be drawn:

(1) For the composite laminated circular panels and shells of revolution with classical boundary conditions, the natural frequencies obtained by using the present method are in quite good agreement with the published results. The results show that the present method enables rapid convergence, high reliability and accuracy.

(2) The vibration characteristics of the composite circular panels and shells of revolution show very large change with the boundary and coupling restraint parameters increasing in the certain range.

(3) The frequency parameters Ω monotonously decrease with the increasing of the circumference angle. In addition, the frequency parameter Ω monotonously increases as the stiffness ratio increases regardless of the structure shapes and boundary conditions. It should be noted that the scope of influence of frequency parameters de-

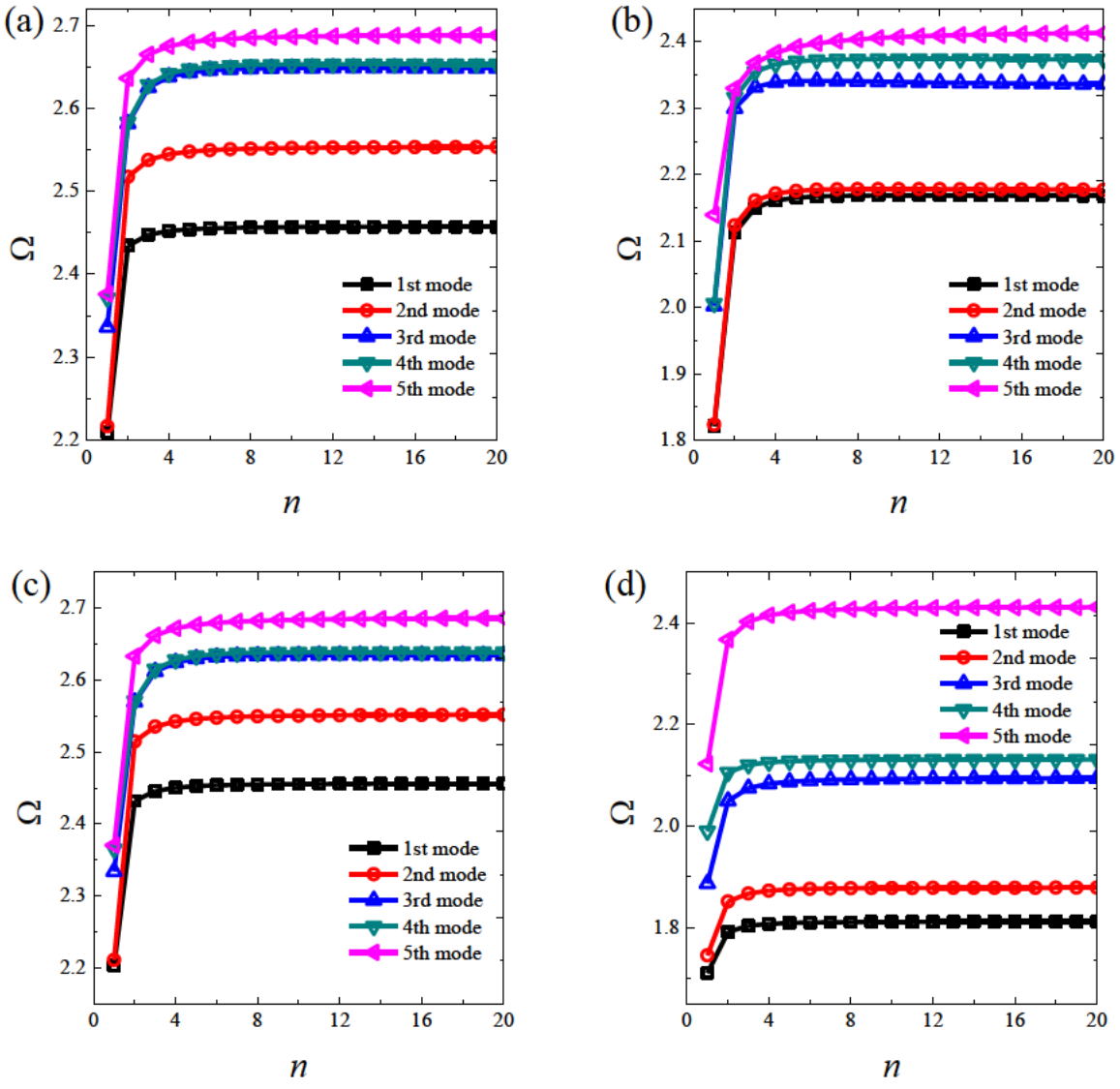

Figure 12: Frequencies of a $[0/90^\circ]_n$ Toro-circular panel ($R_b = 1.5$) with different boundary conditions: (a) CCCC; (b) SSSS; (c) $E^2E^2E^2E^2$; (d) $E^3E^3E^3E^3$.

creases in the same interval region of the stiffness ratio with the stiffness ratio E_1/E_2 increasing

(4) The ply orientations parameters, number of layers and material parameters of the composite laminated circular panels and shells of revolution play a very important role in the mechanic characteristics. For ply orientations parameters: Firstly, all the figures are symmetrical about α=90°; Secondly, there exists obvious differences between the frequency traces of the shell with $[0^\circ/\alpha^\circ]$ lamination and those of $[\alpha^\circ/0^\circ]$. As to the number of layers, the frequency parameters of the structures increase rapidly and may reach their crest around $n = 6$ (12 layer), and beyond this range, the frequency parameters remain unchanged.

(5) In contrast to most existing techniques, the present method can be universally applied to a variety of boundary conditions including all the classical cases, elastic restraints and their combinations without the need of making any change to the solution procedure. Numerous new free vibration results for composite laminated circular panels and shells of revolution with different lamination schemes and elastic restraints are presented.

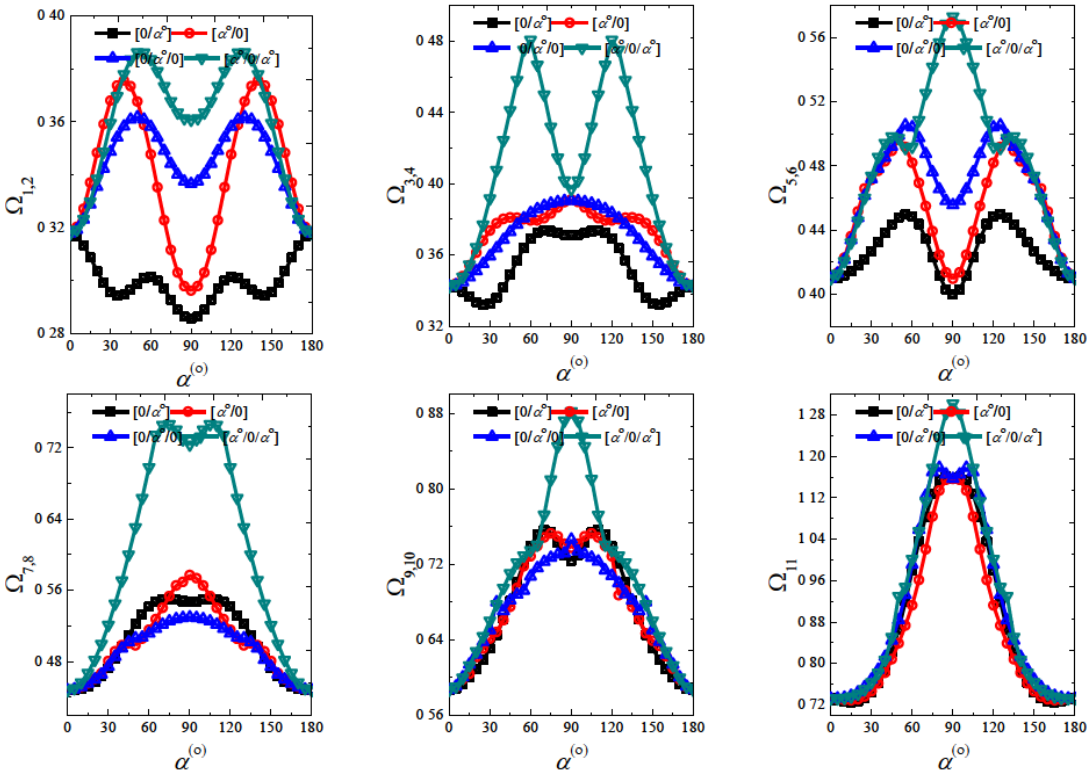

Figure 13: Frequencies of an CF moderately thick composite laminated circular toroid with various lamination schemes.

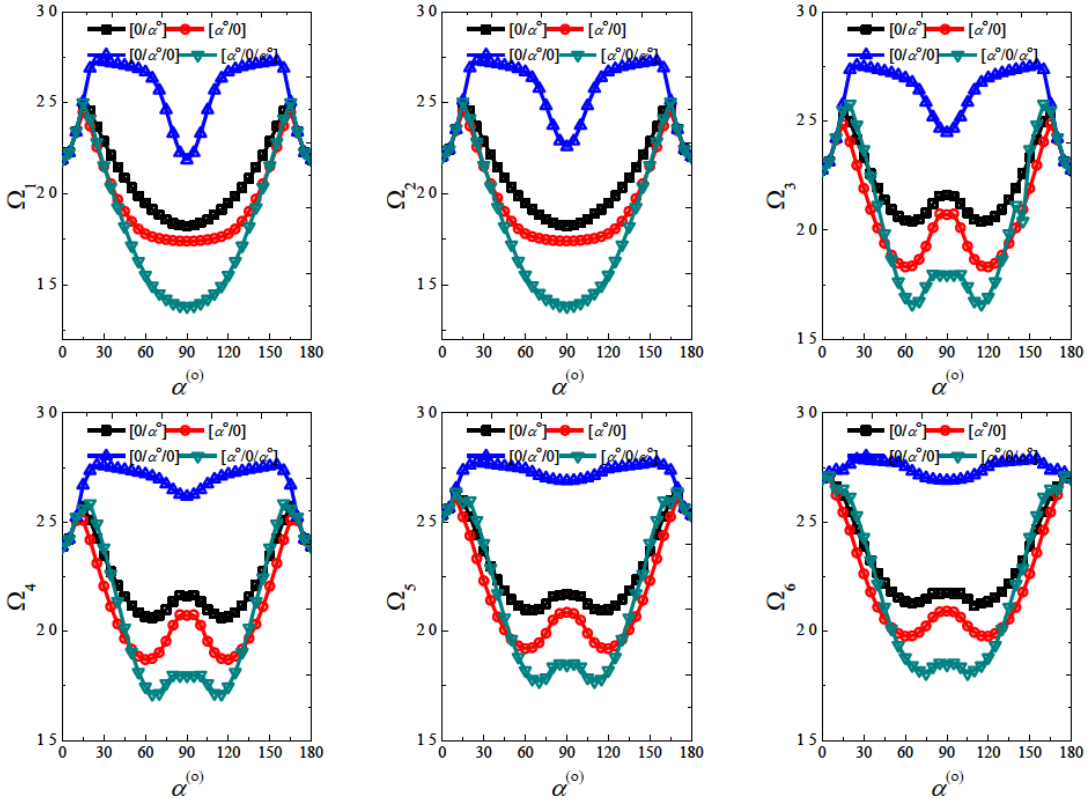

Figure 14: Frequencies of an CFCF moderately thick composite laminated Toro-circular panel with various lamination schemes.

Table 9: The first five frequency parameters Ω for composite laminated circular toroid ($R_b = 1.5$) with different boundary conditions and layouts.

Layout	Mode	Boundary condition								
		CC	CF	SS	SDSD	SF	CS	E^1E^1	E^2E^2	E^3E^3
[0°/90°]	1	2.1568	0.2855	1.7595	0.4259	0.2608	1.8764	1.6824	2.1509	1.6801
	2	2.1631	0.3709	1.7873	0.6690	0.3632	1.8943	1.6834	2.1575	1.6813
	3	2.1944	0.3998	1.7874	1.1199	0.3666	1.9062	1.7118	2.1883	1.7096
	4	2.2264	0.5473	1.8856	1.1398	0.5455	1.9711	1.7451	2.2214	1.7435
	5	2.2861	0.7235	2.0481	1.1843	0.7010	2.0987	1.7665	2.2847	1.7644
[0°/90°/0°]	1	2.4613	0.3366	2.3960	0.4237	0.2452	2.4452	2.0675	2.4610	2.0658
	2	2.7320	0.3905	2.4107	0.6695	0.3498	2.6051	2.1039	2.7312	2.1013
	3	2.8171	0.4555	2.4156	1.1245	0.3547	2.6074	2.1306	2.8162	2.1277
	4	2.8541	0.5298	2.4445	1.2134	0.5201	2.6197	2.1617	2.8532	2.1588
	5	2.8819	0.7461	2.4534	1.2391	0.6884	2.6562	2.2019	2.8810	2.1990
[0°/90°/0°/90°]	1	2.3368	0.3374	2.0570	0.4540	0.2927	2.2095	1.7557	2.3356	1.7525
	2	2.4283	0.4277	2.0572	0.6863	0.3641	2.2159	1.7665	2.4265	1.7632
	3	2.4604	0.4658	2.1128	1.1308	0.4520	2.2488	1.7948	2.4584	1.7926
	4	2.4886	0.6929	2.1238	1.1800	0.6897	2.2678	1.8093	2.4866	1.8059
	5	2.5234	0.7441	2.2415	1.2205	0.7011	2.2748	1.8846	2.5115	1.8813

Table 10: The first five frequency parameters Ω for composite laminated circular toroid ($R_b = -1.5$) with different boundary conditions and layouts.

Layout	Mode	Boundary condition								
		CC	CF	SS	SDSD	SF	CS	E^1E^1	E^2E^2	E^3E^3
[0°/90°]	1	2.2596	0.5962	2.0280	1.0188	0.5793	2.1335	1.7355	2.2548	1.7330
	2	2.4146	0.6000	2.1441	1.6669	0.5923	2.2421	1.9035	2.4099	1.9008
	3	2.6191	1.4943	2.4018	1.7095	1.4913	2.4699	2.2386	2.6155	2.2367
	4	2.8426	2.3539	2.5575	1.9038	2.1985	2.7331	2.7235	2.8373	2.7185
	5	2.9728	2.5648	2.6691	2.0897	2.4226	2.8535	2.8283	2.9670	2.8270
[0°/90°/0°]	1	2.4899	0.5548	2.4331	0.9563	0.5158	2.4584	2.0128	2.4883	2.0105
	2	2.8084	0.6630	2.7411	1.7508	0.5818	2.7638	2.2520	2.8067	2.2489
	3	2.9945	1.2635	2.9327	1.8383	1.2600	2.9524	2.5098	2.9929	2.5070
	4	3.2754	2.1637	3.0561	1.8708	2.1632	3.2233	2.9016	3.2740	2.8993
	5	3.3828	2.5599	3.1852	2.1655	2.4479	3.2418	3.2494	3.3738	3.2422
[0°/90°/0°/90°]	1	2.2978	0.6257	2.1748	1.0305	0.5807	2.2322	1.7729	2.2942	1.7699
	2	2.5232	0.7813	2.3827	1.7061	0.7653	2.4363	2.0039	2.5194	2.0003
	3	2.8897	1.9387	2.7808	1.8039	1.1076	2.8207	2.5149	2.8869	2.5122
	4	3.1349	2.4971	2.8167	1.9055	1.9343	2.9829	2.9686	3.1254	2.9609
	5	3.4192	2.6915	3.1174	2.3635	2.3719	3.2713	3.1395	3.4101	3.1351

Table 11: The first five frequency parameters Ω for composite laminated Toro-circular panel ($R_b = 1.5$) with different boundary conditions and layouts.

Layout	Mode	Boundary condition								
		CCCC	CFCF	SSSS	SDSDSDSD	SFSF	CSCS	$E^1E^1E^1E^1$	$E^2E^2E^2E^2$	$E^3E^3E^3E^3$
[0°/90°]	1	2.2088	1.8129	1.8209	0.8847	1.3238	2.2068	1.7128	2.2030	1.7107
	2	2.2167	1.8129	1.8231	1.1398	1.3238	2.2074	1.7478	2.2110	1.7455
	3	2.3361	2.1349	2.0021	1.2279	1.8036	2.3250	1.8897	2.3341	1.8873
	4	2.3711	2.1883	2.0057	1.2725	1.8322	2.3511	1.9924	2.3654	1.9901
	5	2.3760	2.2132	2.1390	1.4163	1.9650	2.3640	2.1279	2.3706	2.1229
[0°/90°/0°]	1	2.6711	2.1593	2.4329	0.8870	2.1393	2.6549	2.1187	2.6703	2.1163
	2	2.8511	2.5823	2.4337	1.2134	2.1395	2.8399	2.1762	2.8501	2.1733
	3	2.9112	2.6841	2.5052	1.2979	2.1592	2.8974	2.2649	2.9102	2.2621
	4	2.9297	2.6842	2.5537	1.2998	2.4291	2.9279	2.3482	2.9175	2.3454
	5	2.9315	2.7699	2.6235	1.4627	2.4356	2.9297	2.4765	2.9193	2.4740
[0°/90°/0°/90°]	1	2.4341	2.1490	2.1127	0.8976	1.6867	2.4137	1.7950	2.4320	1.7918
	2	2.5172	2.2328	2.1234	1.1800	1.6872	2.4936	1.8555	2.5149	1.8518
	3	2.5813	2.2331	2.2997	1.2927	2.0898	2.5727	2.0540	2.5697	2.0498
	4	2.5831	2.3303	2.3164	1.3015	2.1428	2.5803	2.1084	2.5711	2.1057
	5	2.6361	2.3939	2.3300	1.5338	2.1437	2.5844	2.3714	2.6332	2.3673

Table 12: The first five frequency parameters Ω for composite laminated Toro-circular panel ($R_b = -1.5$) with different boundary conditions and layouts.

Layout	Mode	Boundary condition								
		CCCC	CFCF	SSSS	SDSDSDSD	SFSF	CSCS	$E^1E^1E^1E^1$	$E^2E^2E^2E^2$	$E^3E^3E^3E^3$
[0°/90°]	1	2.8072	1.7885	2.3002	1.6394	1.5342	2.5103	2.3945	2.7989	2.3882
	2	3.3888	1.9473	3.0162	1.9080	1.5829	3.1639	2.8745	3.3819	2.8702
	3	3.5562	1.9718	3.0349	2.0897	1.7319	3.2733	3.1634	3.5456	3.1571
	4	3.9024	2.1600	3.3698	2.6054	1.9145	3.5779	3.2720	3.8911	3.2699
	5	4.7013	2.2434	4.2753	2.6514	2.0766	4.4386	3.8517	4.6902	3.8463
[0°/90°/0°]	1	3.0041	1.8115	2.7836	1.7562	1.8114	2.8468	2.5495	3.0018	2.5464
	2	3.5866	2.5355	3.3220	1.9080	2.2370	3.3734	3.1191	3.5843	3.1163
	3	3.7324	2.6693	3.3503	2.1655	2.2466	3.6241	3.5604	3.7244	3.5536
	4	4.0905	2.6769	3.6854	2.6170	2.4899	3.9396	3.7276	4.0826	3.7215
	5	4.6909	2.7271	4.2515	2.9690	2.6892	4.2835	4.0824	4.6876	4.0808
[0°/90°/0°/90°]	1	3.1249	1.7945	2.6339	1.6961	1.7882	2.7482	2.6656	3.1122	2.6546
	2	3.8595	2.2467	3.3529	1.9080	1.8596	3.6062	3.0508	3.8451	3.0483
	3	4.0712	2.3020	3.7082	2.3635	1.9295	3.7737	3.4158	4.0605	3.4125
	4	4.4237	2.3438	4.0450	2.6301	2.1378	4.2477	3.5904	4.4128	3.5780
	5	5.3687	2.3644	4.8655	2.9855	2.2784	5.2028	4.0902	5.3521	4.0863

Acknowledgement: The authors gratefully acknowledge the financial support from the National Natural Science Foundation of China (No. 51209052).

References

[1] Jin, G., *et al.*, A general Fourier solution for the vibration analysis of composite laminated structure elements of revolution with general elastic restraints. Composite Structures, 2014. 109(0): p. 150–168.

[2] Ye, T., *et al.*, Free vibration analysis of laminated composite shallow shells with general elastic boundaries. Composite Structures, 2013. 106(0): p. 470–490.

[3] Ye, T., *et al.*, A unified Chebyshev–Ritz formulation for vibration analysis of composite laminated deep open shells with arbitrary boundary conditions. Archive of Applied Mechanics, 2014. 84(4): p. 441–471.

[4] Qu, Y., *et al.*, A unified formulation for vibration analysis of composite laminated shells of revolution including shear deformation and rotary inertia. Composite Structures, 2013. 98: p. 169–191.

[5] Ferreira, A., *et al.*, Analysis of laminated doubly-curved shells by a layerwise theory and radial basis functions collocation, accounting for through-the-thickness deformations. Computational Mechanics, 2011. 48(1): p. 13–25.

[6] Ferreira, A., *et al.*, Analysis of laminated shells by a sinusoidal shear deformation theory and radial basis functions collocation, accounting for through-the-thickness deformations. Composites Part B: Engineering, 2011. 42(5): p. 1276–1284.

[7] Chern, Y.-C. and C. Chao, Comparison of natural frequencies of laminates by 3-D theory, part II: curved panels. Journal of sound and vibration, 2000. 230(5): p. 1009–1030.

[8] Singh, B., D. Yadav, and N. Iyengar, Free vibration of laminated spherical panels with random material properties. Journal of sound and vibration, 2001. 244(2): p. 321–338.

[9] Ram, K.S. and T.S. Babu, Free vibration of composite spherical shell cap with and without a cutout. Computers & structures, 2002. 80(23): p. 1749–1756.

[10] Wu, Y., T. Yang, and S. Saigal, Free and forced nonlinear dynamics of composite shell structures. Journal of composite materials, 1987. 21(10): p. 898–909.

[11] Fazzolari, F.A. and E. Carrera, Advances in the Ritz formulation for free vibration response of doubly-curved anisotropic laminated composite shallow and deep shells. Composite Structures, 2013. 101: p. 111–128.

[12] Qatu, M.S., Accurate equations for laminated composite deep thick shells. International Journal of Solids and Structures, 1999. 36(19): p. 2917–2941.

[13] Qatu, M.S., Vibration of laminated shells and plates. 2004: Elsevier.

[14] Kioua, H. and S. Mirza, Piezoelectric induced bending and twisting of laminated composite shallow shells. Smart Materials and Structures, 2000. 9(4): p. 476.

[15] Lal, A., B. Singh, and S. Anand, Nonlinear bending response of laminated composite spherical shell panel with system randomness subjected to hygro-thermo-mechanical loading. International Journal of Mechanical Sciences, 2011. 53(10): p. 855–866.

[16] Lee, S.-Y. and D.-S. Chung, Finite element delamination model for vibrating composite spherical shell panels with central cutouts. Finite elements in analysis and design, 2010. 46(3): p. 247–256.

[17] Mantari, J., A. Oktem, and C.G. Soares, Static and dynamic analysis of laminated composite and sandwich plates and shells by using a new higher-order shear deformation theory. Composite Structures, 2011. 94(1): p. 37–49.

[18] Garg, A.K., R.K. Khare, and T. Kant, Higher-order closed-form solutions for free vibration of laminated composite and sandwich shells. Journal of Sandwich Structures and Materials, 2006. 8(3): p. 205–235.

[19] Panda, S. and B. Singh, Nonlinear free vibration analysis of thermally post-buckled composite spherical shell panel. International Journal of Mechanics and Materials in Design, 2010. 6(2): p. 175–188.

[20] Panda, S.K. and B. Singh, Nonlinear finite element analysis of thermal post-buckling vibration of laminated composite shell panel embedded with SMA fibre. Aerospace Science and Technology, 2013. 29(1): p. 47–57.

[21] Birman, V., S. Griffin, and G. Knowles, Axisymmetric dynamics of composite spherical shells with active piezoelectric/composite stiffeners. Acta Mechanica, 2000. 141(1–2): p. 71–83.

[22] Dasgupta, A. and K. Huang, A layer-wise analysis for free vibrations of thick composite spherical panels. Journal of composite materials, 1997. 31(7): p. 658–671.

[23] Panda, S. and T. Mahapatra, Nonlinear finite element analysis of laminated composite spherical shell vibration under uniform thermal loading. Meccanica, 2014. 49(1): p. 191–213.

[24] Li, W.L., Free vibrations of beams with general boundary conditions. Journal of Sound and Vibration, 2000. 237(4): p. 709–725.

[25] Li, W.L., Dynamic analysis of beams with arbitrary elastic supports at both ends. Journal of Sound and Vibration, 2001. 246(4): p. 751–756.

[26] Li, W.L., Comparison of Fourier sine and cosine series expansions for beams with arbitrary boundary conditions. Journal of Sound and Vibration, 2002. 255(1): p. 185–194.

[27] Du, J., *et al.*, An analytical method for the in-plane vibration analysis of rectangular plates with elastically restrained edges. Journal of Sound and Vibration, 2007. 306(3–5): p. 908–927.

[28] Du, J.T., *et al.*, Free In-Plane Vibration Analysis of Rectangular Plates With Elastically Point-Supported Edges. Journal of Vibration and Acoustics-Transactions of the Asme, 2010. 132(3).

[29] Du, J.T., *et al.*, Acoustic analysis of a rectangular cavity with general impedance boundary conditions. Journal of the Acoustical Society of America, 2011. 130(2): p. 807–17.

[30] Du, J.T., *et al.*, Vibro-acoustic analysis of a rectangular cavity bounded by a flexible panel with elastically restrained edges. Journal of the Acoustical Society of America, 2012. 131(4): p. 2799–810.

[31] Jin, G., *et al.*, An exact solution for the free vibration analysis of laminated composite cylindrical shells with general elastic boundary conditions. Composite Structures, 2013. 106(0): p. 114–127.

[32] Chen, Y., G. Jin, and Z. Liu, Flexural and in-plane vibration analysis of elastically restrained thin rectangular plate with cutout using Chebyshev–Lagrangian method. International Journal of Mechanical Sciences, 2014. 89(0): p. 264–278.

[33] Jin, G., *et al.*, A modified Fourier series solution for vibration analysis of truncated conical shells with general boundary conditions. Applied Acoustics, 2014. 85(0): p. 82–96.

[34] Jin, G., *et al.*, Three-dimensional exact solution for the free vibration of arbitrarily thick functionally graded rectangular plates with general boundary conditions. Composite Structures, 2014. 108(0): p. 565–577.

[35] Jin, G., *et al.*, Three-dimensional vibration analysis of isotropic and orthotropic conical shells with elastic boundary restraints. International Journal of Mechanical Sciences, 2014. 89(0): p. 207–221.

[36] Ma, X., *et al.*, Free and forced vibration analysis of coupled conical–cylindrical shells with arbitrary boundary conditions. International Journal of Mechanical Sciences, 2014. 88(0): p. 122–137.

[37] Su, Z., *et al.*, A unified accurate solution for vibration analysis of arbitrary functionally graded spherical shell segments with general end restraints. Composite Structures, 2014. 111(0): p. 271–284.

[38] Su, Z., *et al.*, A unified solution for vibration analysis of functionally graded cylindrical, conical shells and annular plates with general boundary conditions. International Journal of Mechanical Sciences, 2014. 80(0): p. 62–80.

[39] Su, Z., G. Jin, and T. Ye, Three-dimensional vibration analysis of thick functionally graded conical, cylindrical shell and annular plate structures with arbitrary elastic restraints. Composite Structures, 2014. 118(0): p. 432–447.

[40] Su, Z., G. Jin, and T. Ye, Free vibration analysis of moderately thick functionally graded open shells with general boundary conditions. Composite Structures, 2014. 117(0): p. 169–186.

[41] Ye, T., *et al.*, A unified formulation for vibration analysis of open shells with arbitrary boundary conditions. International Journal of Mechanical Sciences, 2014. 81(0): p. 42–59.

[42] Ye, T., *et al.*, Three-dimensional free vibration analysis of thick cylindrical shells with general end conditions and resting on elastic foundations. International Journal of Mechanical Sciences, 2014. 84(0): p. 120–137.

[43] Ye, T., G. Jin, and Z. Su, Three-dimensional vibration analysis of laminated functionally graded spherical shells with general boundary conditions. Composite Structures, 2014. 116(0): p. 571–588.

[44] Ye, T., *et al.*, A modified Fourier solution for vibration analysis of moderately thick laminated plates with general boundary restraints and internal line supports. International Journal of Mechanical Sciences, 2014. 80(0): p. 29–46.

[45] Jin, G., *et al.*, A modified Fourier–Ritz approach for free vibration analysis of laminated functionally graded shallow shells with general boundary conditions. International Journal of Mechanical Sciences, 2015. 93(0): p. 256–269.

[46] Yang, C., *et al.*, Vibration and damping analysis of thick sandwich cylindrical shells with a viscoelastic core under arbitrary boundary conditions. International Journal of Mechanical Sciences, 2015. 92(0): p. 162–177.

[47] Shi, D., *et al.*, Free Vibration Analysis of Moderately Thick Rectangular Plates with Variable Thickness and Arbitrary Boundary Conditions. Shock and Vibration, 2014. 2014.

[48] Shi, D., *et al.*, An accurate solution method for the vibration analysis of Timoshenko beams with general elastic supports. Proceedings of the Institution of Mechanical Engineers, Part C: Journal of Mechanical Engineering Science, 2014: p. 0954406214558675.

[49] Shi, D., *et al.*, A series solution for the in-plane vibration analysis of orthotropic rectangular plates with non-uniform elastic boundary constraints and internal line supports. Archive of Applied Mechanics, 2015. 85(1): p. 51–73.

[50] Wang, Q., D. Shi, and Q. Liang, Free vibration analysis of axially loaded laminated composite beams with general boundary conditions by using a modified Fourier–Ritz approach. Journal of Composite Materials, 2015: p. 0021998315602138.

[51] Wang, Q., D. Shi, and X. Shi, A modified solution for the free vibration analysis of moderately thick orthotropic rectangular plates with general boundary conditions, internal line supports and resting on elastic foundation. Meccanica: p. 1–33.

[52] Wang, Q., *et al.*, A unified solution for vibration analysis of functionally graded circular, annular and sector plates with general boundary conditions. Composites Part B: Engineering, 2015.

[53] Tornabene, F. and E. Viola, Free vibration analysis of functionally graded panels and shells of revolution. Meccanica, 2009. 44(3): p. 255–281.

[54] Tornabene, F. and E. Viola, Free vibrations of four-parameter functionally graded parabolic panels and shells of revolution. European Journal of Mechanics-A/Solids, 2009. 28(5): p. 991–1013.

[55] Tornabene, F., 2-D GDQ solution for free vibrations of anisotropic doubly-curved shells and panels of revolution. Composite Structures, 2011. 93(7): p. 1854–1876.

[56] Du, J., *et al.*, Free vibration of two elastically coupled rectangular plates with uniform elastic boundary restraints. Journal of Sound and Vibration, 2011. 330(4): p. 788–804.

Appendix A. Detailed expressions of the lamina stiffness coefficients

$$\overline{Q}_{11}^{k} = Q_{11}^{k}\cos^4\alpha^k + 2\left(Q_{12}^{k} + 2Q_{66}^{k}\right)\sin^2\alpha^k\cos^2\theta^k + Q_{22}^{k}\sin^4\alpha^k \tag{A.1}$$

$$\overline{Q}_{12}^{k} = \left(Q_{11}^{k} + Q_{22}^{k} - 4Q_{66}^{k}\right)\sin^2\alpha^k\cos^2\theta^k + Q_{12}^{k}\left(\sin^4\alpha^k + \cos^4\alpha^k\right) \tag{A.2}$$

$$\overline{Q}_{12}^{k} = \left(Q_{11}^{k} + Q_{22}^{k} - 4Q_{66}^{k}\right)\sin^2\alpha^k\cos^2\alpha^k + Q_{12}^{k}\left(\sin^4\alpha^k + \cos^4\alpha^k\right) \tag{A.3}$$

$$\overline{Q}_{16}^{k} = \left(Q_{11}^{k} - Q_{12}^{k} - 2Q_{66}^{k}\right)\cos^3\alpha^k\sin\alpha^k + \left(Q_{12}^{k} - Q_{22}^{k} + 2Q_{66}^{k}\right)\sin^3\alpha^k\cos\alpha^k \tag{A.4}$$

$$\overline{Q}_{26}^{k} = \left(Q_{11}^{k} - Q_{12}^{k} - 2Q_{66}^{k}\right)\sin^3\alpha^k\cos\alpha^k + \left(Q_{12}^{k} - Q_{22}^{k} + 2Q_{66}^{k}\right)\cos^3\alpha^k\sin\alpha^k \tag{A.5}$$

$$\overline{Q}_{66}^{k} = \left(Q_{11}^{k} + Q_{22}^{k} - 2Q_{66}^{k}\right)\sin^2\alpha^k\cos^2\alpha^k + Q_{66}^{k}\left(\sin^4\alpha^k + \cos^4\alpha^k\right) \tag{A.6}$$

$$\overline{Q}_{44}^{k} = Q_{44}^{k}\cos^2\alpha^k + Q_{55}^{k}\sin^2\alpha^k \tag{A.7}$$

$$\overline{Q}_{55}^{k} = Q_{55}^{k}\cos^2\alpha^k + Q_{44}^{k}\sin^2\alpha^k \tag{A.8}$$

$$\overline{Q}_{45}^{k} = \left(Q_{55}^{k} - Q_{44}^{k}\right)\cos\alpha^k\sin\alpha^k \tag{A.9}$$

where α^k is the fiber orientation angle between the principal direction of the $k^{'}$th orthotropic lamina layer and the φ-direction. The Q_{ij} are the plane-stress reduced elastic constants in the material axes of the th orthotropic lamina:

$$Q_{11}^{k} = \frac{E_1^k}{1-\mu_{12}^k\mu_{21}^k},\ Q_{22}^{k} = \frac{E_2^k}{1-\mu_{12}^k\mu_{21}^k},\ Q_{12}^{k} = Q_{21}^{k} = \mu_{21}^k Q_{11}^{k} \tag{A.10}$$

$$Q_{33}^{k} = G_{12}^{k},\ Q_{44}^{k} = G_{23}^{k},\ Q_{55}^{k} = G_{13}^{k},\ \mu_{21}^{k} = \mu_{12}^{k}\frac{E_2^k}{E_1^k} \tag{A.11}$$

in which E_1, E_2, μ_{12}, μ_{12}, G_{12}, G_{23} and G_{13} are the material properties of the th orthotropic lamina.

Appendix B. Detailed expressions of the matrices M, K and H

$$\mathbf{K} = \begin{bmatrix} \mathbf{K}_{uu} & \mathbf{K}_{uv} & \mathbf{K}_{uw} & \mathbf{K}_{u\varphi} & \mathbf{K}_{u\theta} \\ \mathbf{K}_{uv}^T & \mathbf{K}_{vv} & \mathbf{K}_{vw} & \mathbf{K}_{v\varphi} & \mathbf{K}_{v\theta} \\ \mathbf{K}_{uw}^T & \mathbf{K}_{vw}^T & \mathbf{K}_{ww} & \mathbf{K}_{w\varphi} & \mathbf{K}_{w\theta} \\ \mathbf{K}_{u\varphi}^T & \mathbf{K}_{v\varphi}^T & \mathbf{K}_{w\varphi}^T & \mathbf{K}_{\varphi\varphi} & \mathbf{K}_{\varphi\theta} \\ \mathbf{K}_{u\theta}^T & \mathbf{K}_{v\theta}^T & \mathbf{K}_{w\theta}^T & \mathbf{K}_{\varphi\theta} & \mathbf{K}_{\theta\theta} \end{bmatrix}, \tag{B.1}$$

$$\mathbf{M} = \begin{bmatrix} \mathbf{M}_{uu} & \mathbf{0} & \mathbf{0} & \mathbf{M}_{u\varphi} & \mathbf{0} \\ \mathbf{0} & \mathbf{M}_{vv} & \mathbf{0} & \mathbf{0} & \mathbf{M}_{v\theta} \\ \mathbf{0} & \mathbf{0} & \mathbf{M}_{ww} & \mathbf{0} & \mathbf{0} \\ \mathbf{M}_{u\varphi}^T & \mathbf{0} & \mathbf{0} & \mathbf{M}_{\varphi\varphi} & \mathbf{0} \\ \mathbf{0} & \mathbf{M}_{v\theta}^T & \mathbf{0} & \mathbf{0} & \mathbf{M}_{\theta\theta} \end{bmatrix}, \tag{B.2}$$

$$\mathbf{H} = \begin{pmatrix} \mathbf{H}_u \\ \mathbf{H}_v \\ \mathbf{H}_w \\ \mathbf{H}_\varphi \\ \mathbf{H}_\theta \end{pmatrix} \tag{B.3}$$

$$\begin{aligned} \mathbf{K}_{uu} = & \int\int \left\{ \begin{array}{l} A_{11}\frac{R_0}{R_\varphi}\frac{\partial \mathbf{U}^T}{\partial\varphi}\frac{\partial \mathbf{U}}{\partial\varphi} + A_{22}\frac{R_\varphi c_\varphi^2}{R_0}\mathbf{U}^T\mathbf{U} + \kappa A_{55}\frac{R_0}{R_\varphi}\mathbf{U}^T\mathbf{U} \\ +A_{66}\frac{R_\varphi}{R_0}\frac{\partial \mathbf{U}^T}{\partial\theta}\frac{\partial \mathbf{U}}{\partial\theta} + A_{12}c_\varphi\left(\frac{\partial \mathbf{U}^T}{\partial\varphi}\mathbf{U} + \mathbf{U}^T\frac{\partial \mathbf{U}}{\partial\varphi}\right) \\ +A_{16}\left(\frac{\partial \mathbf{U}^T}{\partial\varphi}\frac{\partial \mathbf{U}}{\partial\theta} + \frac{\partial \mathbf{U}^T}{\partial\theta}\frac{\partial \mathbf{U}}{\partial\varphi}\right) + A_{26}\frac{R_\varphi}{R_0}c_\varphi c_\varphi\left(\mathbf{U}^T\frac{\partial \mathbf{U}}{\partial\theta} + \frac{\partial \mathbf{U}^T}{\partial\theta}\mathbf{U}\right) \end{array} \right\} dS \\ & + \int\int \left\{k^u_{\varphi 0}\mathbf{U}^T\mathbf{U}\right\}_{|\varphi=\varphi_0} dS_0 + \int\int \left\{k^u_{\varphi 1}\mathbf{U}^T\mathbf{U}\right\}_{|\varphi=\varphi_1} dS_1 + \int\int \left\{k^u_{\theta 0}\mathbf{U}^T\mathbf{U}\right\}_{|\theta=0} dS_2 \\ & + \int\int \left\{k^u_{\theta 1}\mathbf{U}^T\mathbf{U}\right\}_{|\theta=\phi} dS_3 + \int\int \left\{k^u_{uc}\left(\mathbf{U}_{|\theta=0} - \mathbf{U}_{|\phi=2\pi}\right)^T\left(\mathbf{U}_{|\theta=0} - \mathbf{U}_{|\phi=2\pi}\right)\right\} dS_2 \end{aligned} \tag{B.4}$$

$$\mathbf{K}_{uv} = \int\int \left\{ \begin{array}{l} A_{22}\frac{R_\varphi c_\varphi}{R_0}\left(\frac{\partial \mathbf{V}^T}{\partial\theta}\mathbf{U} + \frac{\partial \mathbf{V}}{\partial\theta}\mathbf{U}^T\right) + A_{66}\left(\frac{\partial \mathbf{V}^T}{\partial\varphi}\frac{\partial \mathbf{U}}{\partial\theta} + \frac{\partial \mathbf{V}}{\partial\varphi}\frac{\partial \mathbf{U}^T}{\partial\theta}\right) \\ +A_{12}\left(\frac{\partial \mathbf{U}^T}{\partial\varphi}\frac{\partial \mathbf{V}}{\partial\theta} + \frac{\partial \mathbf{U}}{\partial\varphi}\frac{\partial \mathbf{V}^T}{\partial\theta}\right) + A_{16}\frac{R_0}{R_\varphi}\left(\frac{\partial \mathbf{U}^T}{\partial\varphi}\frac{\partial \mathbf{V}}{\partial\varphi} + \frac{\partial \mathbf{U}}{\partial\varphi}\frac{\partial \mathbf{V}^T}{\partial\varphi}\right) \\ -A_{16}c_\varphi\left(\frac{\partial \mathbf{U}^T}{\partial\varphi}\mathbf{V} + \frac{\partial \mathbf{U}}{\partial\varphi}\mathbf{V}^T\right) + A_{26}c_\varphi\left(\mathbf{U}^T\frac{\partial \mathbf{V}}{\partial\varphi} + \mathbf{U}\frac{\partial \mathbf{V}^T}{\partial\varphi}\right) \\ -A_{26}c_\varphi^2\left(\partial\mathbf{U}^T\mathbf{V} + \mathbf{U}\mathbf{V}^T\right) + A_{26}\frac{R_\varphi}{R_0}\left(\frac{\partial \mathbf{U}^T}{\partial\theta}\frac{\partial \mathbf{V}}{\partial\theta} + \frac{\partial \mathbf{U}}{\partial\theta}\frac{\partial \mathbf{V}^T}{\partial\theta}\right) \\ +\kappa A_{45}s_\varphi\left(\mathbf{U}^T\mathbf{V} + \mathbf{U}\mathbf{V}^T\right) \end{array} \right\} dS \tag{B.5}$$

$$\mathbf{K}_{uw} = \int\int \left\{ \begin{array}{l} A_{11}\frac{R_0}{R_\varphi}\left(\frac{\partial \mathbf{U}^T}{\partial\varphi}\mathbf{W} + \mathbf{W}^T\frac{\partial \mathbf{U}}{\partial\varphi}\right) + A_{22}\frac{R_\varphi}{R_0}c_\varphi s_\varphi\left(\mathbf{U}^T\mathbf{W} + \mathbf{W}^T\mathbf{U}\right) \\ +\kappa A_{55}\frac{R_0}{R_\varphi}\left(\frac{\partial \mathbf{W}^T}{\partial\varphi}\mathbf{U} + \mathbf{U}^T\frac{\partial \mathbf{W}}{\partial\varphi}\right) + A_{12}s_\varphi\left(\frac{\partial \mathbf{U}^T}{\partial\varphi}\mathbf{W} + \mathbf{W}^T\frac{\partial \mathbf{U}}{\partial\varphi}\right) \\ +A_{12}c_\varphi\left(\mathbf{U}^T\mathbf{W} + \mathbf{W}^T\mathbf{U}\right) + A_{26}s_\varphi\frac{R_\varphi}{R_0}\left(\frac{\partial \mathbf{U}^T}{\partial\theta}\mathbf{W} + \mathbf{W}^T\frac{\partial \mathbf{U}}{\partial\theta}\right) \\ -\kappa A_{45}\left(\frac{\partial \mathbf{W}^T}{\partial\theta}\mathbf{U} + \mathbf{U}^T\frac{\partial \mathbf{W}}{\partial\theta}\right) \end{array} \right\} dS \tag{B.6}$$

$$\mathbf{K}_{u\varphi} = \int\int \left\{ \begin{array}{l} B_{11}\frac{R_0}{R_\varphi}\left(\frac{\partial \mathbf{U}^T}{\partial\varphi}\frac{\partial \boldsymbol{\Phi}}{\partial\varphi} + \frac{\partial \mathbf{U}}{\partial\varphi}\frac{\partial \boldsymbol{\Phi}^T}{\partial\varphi}\right) + B_{12}c_\varphi\left(\frac{\partial \mathbf{U}^T}{\partial\varphi}\boldsymbol{\Phi} + \frac{\partial \mathbf{U}}{\partial\varphi}\boldsymbol{\Phi}^T\right) \\ +B_{16}c_\varphi^2\frac{\partial \mathbf{U}^T}{\partial\varphi}\frac{\partial \boldsymbol{\Phi}}{\partial\theta} + \frac{\partial \mathbf{U}}{\partial\varphi}\frac{\partial \boldsymbol{\Phi}^T}{\partial\theta} + B_{12}c_\varphi\left(\mathbf{U}^T\frac{\partial \boldsymbol{\Phi}}{\partial\varphi} + \mathbf{U}\frac{\partial \boldsymbol{\Phi}^T}{\partial\varphi}\right) \\ +B_{22}\frac{R_\varphi}{R_0}c_\varphi^2\left(\mathbf{U}^T\boldsymbol{\Phi} + \mathbf{U}\boldsymbol{\Phi}^T\right) + B_{26}\frac{R_\varphi}{R_0}c_\varphi\left(\mathbf{U}^T\frac{\partial \boldsymbol{\Phi}}{\partial\theta} + \mathbf{U}\frac{\partial \boldsymbol{\Phi}^T}{\partial\theta}\right) \\ +B_{16}c_\varphi\left(\frac{\partial \mathbf{U}^T}{\partial\theta}\frac{\partial \boldsymbol{\Phi}}{\partial\varphi} + \frac{\partial \mathbf{U}}{\partial\theta}\frac{\partial \boldsymbol{\Phi}^T}{\partial\varphi}\right) + B_{26}\frac{R_\varphi}{R_0}c_\varphi\left(\frac{\partial \mathbf{U}^T}{\partial\theta}\boldsymbol{\Phi} + \frac{\partial \mathbf{U}}{\partial\theta}\boldsymbol{\Phi}^T\right) \\ B_{66}\frac{R_\varphi}{R_0}c_\varphi\left(\frac{\partial \mathbf{U}^T}{\partial\theta}\frac{\partial \boldsymbol{\Phi}}{\partial\varphi} + \frac{\partial \mathbf{U}}{\partial\theta}\frac{\partial \boldsymbol{\Phi}^T}{\partial\varphi}\right) \end{array} \right\} dS \tag{B.7}$$

$$\mathbf{K}_{u\theta} = \int\int \left\{ \begin{array}{l} B_{12}\left(\frac{\partial \mathbf{U}^T}{\partial\varphi}\frac{\partial \boldsymbol{\Theta}}{\partial\theta} + \frac{\partial \mathbf{U}}{\partial\varphi}\frac{\partial \boldsymbol{\Theta}^T}{\partial\theta}\right) - B_{16}c_\varphi\left(\frac{\partial \mathbf{U}^T}{\partial\varphi}\boldsymbol{\Theta} + \frac{\partial \mathbf{U}}{\partial\varphi}\boldsymbol{\Theta}^T\right) \\ +B_{16}c_\varphi\frac{R_0}{R_\varphi}\left(\frac{\partial \mathbf{U}^T}{\partial\varphi}\frac{\partial \boldsymbol{\Theta}}{\partial\varphi} + \frac{\partial \mathbf{U}}{\partial\varphi}\frac{\partial \boldsymbol{\Theta}^T}{\partial\varphi}\right) + B_{22}c_\varphi\frac{R_0}{R_\varphi}\left(\mathbf{U}^T\frac{\partial \boldsymbol{\Theta}}{\partial\theta} + \mathbf{U}\frac{\partial \boldsymbol{\Theta}^T}{\partial\theta}\right) \\ +B_{26}c_\varphi\frac{R_0}{R_\varphi}\left(\mathbf{U}^T\frac{\boldsymbol{\Theta}}{\partial\varphi} + \mathbf{U}\frac{\boldsymbol{\Theta}^T}{\partial\varphi}\right) - B_{26}c_\varphi^2\frac{R_\varphi}{R_0}\left(\mathbf{U}^T\partial\boldsymbol{\Theta} + \mathbf{U}\partial\boldsymbol{\Theta}^T\right) \\ +B_{26}\frac{R_\varphi}{R_0}\left(\frac{\partial \mathbf{U}^T}{\partial\theta}\frac{\partial \boldsymbol{\Theta}}{\partial\theta} + \frac{\partial \mathbf{U}}{\partial\theta}\frac{\partial \boldsymbol{\Theta}^T}{\partial\theta}\right) + B_{26}\left(\frac{\partial \mathbf{U}^T}{\partial\theta}\frac{\boldsymbol{\Theta}}{\partial\varphi} + \frac{\partial \mathbf{U}}{\partial\theta}\frac{\boldsymbol{\Theta}^T}{\partial\varphi}\right) \\ -B_{66}c_\varphi\frac{R_\varphi}{R_0}\left(\frac{\partial \mathbf{U}^T}{\partial\theta}\boldsymbol{\Theta} + \frac{\partial \mathbf{U}}{\partial\theta}\boldsymbol{\Theta}^T\right) \end{array} \right\} dS \tag{B.8}$$

$$\begin{aligned} \mathbf{K}_{vv} = & \int\int \left\{ \begin{array}{l} A_{22}\frac{R_\varphi}{R_0}\frac{\partial \mathbf{V}^T}{\partial\theta}\frac{\partial \mathbf{V}}{\partial\theta} + A_{66}\left(\frac{R_0\partial \mathbf{V}^T}{\partial\varphi} - c_\varphi R_\varphi\mathbf{V}^T\right)\left(\frac{\partial \mathbf{V}}{R_\varphi\partial\varphi} - c_\varphi\frac{\mathbf{V}}{R_0}\right) \\ +\kappa A_{44}\frac{R_\varphi s_\varphi^2}{R_0}\mathbf{V}^T\mathbf{V} + A_{26}\left(\frac{\partial \mathbf{V}^T}{\partial\theta}\frac{\partial \mathbf{V}}{\partial\varphi} + \frac{\partial \mathbf{V}^T}{\partial\varphi}\frac{\partial \mathbf{V}}{\partial\theta}\right) - A_{26}\frac{R_\varphi}{R_0}c_\varphi\left(\frac{\partial \mathbf{V}^T}{\partial\theta}\mathbf{V} + \mathbf{V}^T\frac{\partial \mathbf{V}}{\partial\theta}\right) \end{array} \right\} dS \\ & \int\int \left\{k^v_{\varphi 0}\mathbf{V}^T\mathbf{V}\right\}_{|\varphi=\varphi_0} dS_0 + \int\int \left\{k^v_{\varphi 1}\mathbf{V}^T\mathbf{V}\right\}_{|\theta=\theta_1} dS_1 + \int\int \left\{k^v_{\theta 0}\mathbf{V}^T\mathbf{V}\right\}_{|\theta=0} dS_2 \end{aligned} \tag{B.9}$$

$$+\int\int\left\{k_{\theta1}^{v}\mathbf{V}^{T}\mathbf{V}\right\}_{|\theta=\phi}dS_3+\int\int\left\{k_{uc}^{v}\left(\mathbf{V}_{|\theta=0}-\mathbf{V}_{|\phi=2\pi}\right)^{T}\left(\mathbf{V}_{|\theta=0}-\mathbf{V}_{|\phi=2\pi}\right)\right\}dS_2$$

$$\mathbf{K}_{vw}=\int\int\left\{\begin{array}{l}A_{22}\frac{R_\varphi s_\varphi}{R_0}\left(\frac{\partial\mathbf{V}^T}{\partial\theta}\mathbf{W}+\mathbf{W}^T\frac{\partial\mathbf{V}}{\partial\theta}\right)-\kappa A_{44}\left(\mathbf{V}^T\frac{\partial\mathbf{W}}{\partial\theta}+\mathbf{V}\frac{\partial\mathbf{W}^T}{\partial\theta}\right)\\+A_{12}\left(\frac{\partial\mathbf{V}^T}{\partial\theta}\mathbf{W}+\mathbf{W}^T\frac{\partial\mathbf{V}}{\partial\theta}\right)+A_{16}\frac{R_0}{R_\varphi}\left(\frac{\partial\mathbf{V}^T}{\partial\varphi}\mathbf{W}+\mathbf{W}^T\frac{\partial\mathbf{V}}{\partial\varphi}\right)\\+A_{26}\left(\frac{1}{R_\varphi}\frac{\partial\mathbf{V}^T}{\partial\varphi}-\frac{1}{R_0}c_\varphi\mathbf{V}^T\right)\mathbf{W}s_\varphi+A_{26}\left(\frac{1}{R_\varphi}\frac{\partial\mathbf{V}}{\partial\varphi}-\frac{1}{R_0}c_\varphi\mathbf{V}\right)\mathbf{W}^Ts_\varphi\\-\kappa A_{45}s_\varphi\left(\frac{\partial\mathbf{W}^T}{\partial\varphi}\mathbf{V}+\mathbf{V}^T\frac{\partial\mathbf{W}}{\partial\varphi}\right)\end{array}\right\}dS \tag{B.10}$$

$$\mathbf{K}_{v\varphi}=\int\int\left\{\begin{array}{l}\kappa A_{45}R_\varphi s_\varphi\left(\boldsymbol{\Phi}\mathbf{V}^T+\boldsymbol{\Phi}^T\mathbf{V}\right)+B_{12}c_\varphi\left(\frac{\partial\mathbf{V}^T}{\partial\theta}\frac{\partial\boldsymbol{\Phi}}{\partial\varphi}+\frac{\partial\boldsymbol{\Phi}^T}{\partial\varphi}\frac{\partial\mathbf{V}}{\partial\theta}\right)\\+B_{22}c_\varphi\frac{R_\varphi}{R_0}\left(\frac{\partial\mathbf{V}^T}{\partial\theta}\boldsymbol{\Phi}+\boldsymbol{\Phi}^T\frac{\partial\mathbf{V}}{\partial\theta}\right)+B_{26}\frac{R_\varphi}{R_0}\left(\frac{\partial\mathbf{V}^T}{\partial\theta}\frac{\partial\boldsymbol{\Phi}}{\partial\theta}+\frac{\partial\boldsymbol{\Phi}^T}{\partial\theta}\frac{\partial\mathbf{V}}{\partial\theta}\right)\\+B_{16}\left(\left(\frac{1}{R_\varphi}\frac{\partial\mathbf{V}^T}{\partial\theta}-\frac{1}{R_0}\mathbf{V}^T\right)\frac{\partial\boldsymbol{\Phi}}{\partial\varphi}+\frac{\partial\boldsymbol{\Phi}^T}{\partial\varphi}\left(\frac{1}{R_\varphi}\frac{\partial\mathbf{V}}{\partial\theta}-\frac{1}{R_0}\mathbf{V}\right)\right)\\+B_{26}c_\varphi R_\varphi R_0\left(\left(\frac{1}{R_\varphi}\frac{\partial\mathbf{V}^T}{\partial\theta}-\frac{1}{R_0}\mathbf{V}^T\right)\boldsymbol{\Phi}+\boldsymbol{\Phi}^T\left(\frac{1}{R_\varphi}\frac{\partial\mathbf{V}}{\partial\theta}-\frac{1}{R_0}\mathbf{V}\right)\right)\\+B_{66}c_\varphi R_\varphi\left(\left(\frac{1}{R_\varphi}\frac{\partial\mathbf{V}^T}{\partial\theta}-\frac{1}{R_0}\mathbf{V}^T\right)\frac{\partial\boldsymbol{\Phi}}{\partial\theta}+\frac{\partial\boldsymbol{\Phi}^T}{\partial\theta}\left(\frac{1}{R_\varphi}\frac{\partial\mathbf{V}}{\partial\theta}-\frac{1}{R_0}\mathbf{V}\right)\right)\end{array}\right\}dS \tag{B.11}$$

$$\mathbf{K}_{v\theta}=\int\int\left\{\begin{array}{l}-\kappa A_{44}R_\varphi s_\varphi\left(\mathbf{V}^T\boldsymbol{\Phi}+\boldsymbol{\Phi}^T\mathbf{V}\right)+B_{22}\frac{R_\varphi}{R_0}\left(\frac{\partial\mathbf{V}^T}{\partial\theta}\frac{\partial\boldsymbol{\Phi}}{\partial\theta}+\frac{\partial\boldsymbol{\Phi}^T}{\partial\theta}\frac{\partial\mathbf{V}}{\partial\theta}\right)\\+B_{26}\left(\frac{\partial\mathbf{V}^T}{\partial\theta}\frac{\partial\boldsymbol{\Phi}}{\partial\varphi}+\frac{\partial\boldsymbol{\Phi}^T}{\partial\varphi}\frac{\partial\mathbf{V}}{\partial\theta}\right)-B_{26}c_\varphi\frac{R_\varphi}{R_0}\left(\frac{\partial\mathbf{V}^T}{\partial\theta}\boldsymbol{\Phi}+\boldsymbol{\Phi}^T\frac{\partial\mathbf{V}}{\partial\theta}\right)\\+B_{26}\left(\frac{\partial\mathbf{V}^T}{\partial\varphi}\frac{\partial\boldsymbol{\Phi}}{\partial\theta}+\frac{\partial\boldsymbol{\Phi}^T}{\partial\theta}\frac{\partial\mathbf{V}}{\partial\varphi}\right)-B_{26}c_\varphi\frac{R_\varphi}{R_0}\left(\mathbf{V}^T\frac{\partial\boldsymbol{\Phi}}{\partial\theta}+\frac{\partial\boldsymbol{\Phi}^T}{\partial\theta}\mathbf{V}\right)\\+B_{66}\frac{R_0}{R_\varphi}\left(\frac{\partial\mathbf{V}^T}{\partial\varphi}\frac{\partial\boldsymbol{\Phi}}{\partial\varphi}+\frac{\partial\boldsymbol{\Phi}^T}{\partial\varphi}\frac{\partial\mathbf{V}}{\partial\varphi}\right)-B_{66}c_\varphi\left(\frac{\mathbf{V}^T}{\partial\varphi}\boldsymbol{\Phi}+\boldsymbol{\Phi}^T\frac{\partial\mathbf{V}}{\partial\varphi}\right)\\-B_{66}c_\varphi\left(\mathbf{V}^T\frac{\partial\boldsymbol{\Phi}}{\partial\varphi}+\frac{\partial\boldsymbol{\Phi}^T}{\partial\varphi}\mathbf{V}\right)+B_{66}c_\varphi^2\frac{R_\varphi}{R_0}\left(\mathbf{V}^T\boldsymbol{\Phi}+\boldsymbol{\Phi}^T\mathbf{V}\right)\end{array}\right\}dS \tag{B.12}$$

$$\mathbf{K}_{ww}=\int\int\left\{\begin{array}{l}A_{11}\frac{R_0}{R_\varphi}\mathbf{W}^T\mathbf{W}+A_{11}\frac{R_\varphi}{R_0}s_\varphi^2\mathbf{W}^T\mathbf{W}+\kappa A_{55}\frac{R_0}{R_\varphi}\frac{\partial\mathbf{W}^T}{\partial\varphi}\frac{\partial\mathbf{W}}{\partial\varphi}\\+A_{12}s_\varphi\mathbf{W}^T\mathbf{W}+\kappa A_{44}\frac{R_\varphi}{R_0}\frac{\partial\mathbf{W}^T}{\partial\theta}\frac{\partial\mathbf{W}}{\partial\theta}+\kappa A_{45}\left(\frac{\partial\mathbf{W}^T}{\partial\varphi}\frac{\partial\mathbf{W}}{\partial\theta}+\frac{\partial\mathbf{W}^T}{\partial\theta}\frac{\partial\mathbf{W}}{\partial\varphi}\right)\end{array}\right\}dS \tag{B.13}$$
$$+\int\int\left\{k_{\varphi0}^{w}\mathbf{W}^T\mathbf{W}\right\}_{|\varphi=\varphi_0}dS_0+\int\int\left\{k_{\varphi1}^{w}\mathbf{W}^T\mathbf{W}\right\}_{|\varphi=\varphi_1}dS_1+\int\int\left\{k_{\theta0}^{w}\mathbf{W}^T\mathbf{W}\right\}_{|\theta=0}dS_2$$
$$+\int\int\left\{k_{\theta1}^{w}\mathbf{W}^T\mathbf{W}\right\}_{|\theta=\phi}dS_3+\int\int\left\{k_{uc}^{w}\left(\mathbf{W}_{|\theta=0}-\mathbf{W}_{|\phi=2\pi}\right)^{T}\left(\mathbf{W}_{|\theta=0}-\mathbf{W}_{|\phi=2\pi}\right)\right\}dS_2$$

$$\mathbf{K}_{w\varphi}=\int\int\left\{\begin{array}{l}\kappa A_{55}R_0\left(\frac{\partial\mathbf{W}^T}{\partial\varphi}\boldsymbol{\Phi}+\frac{\partial\mathbf{W}}{\partial\varphi}\boldsymbol{\Phi}^T\right)+B_{11}\frac{R_0}{R_\varphi}\left(\frac{\partial\boldsymbol{\Phi}^T}{\partial\varphi}\mathbf{W}+\frac{\partial\boldsymbol{\Phi}}{\partial\varphi}\mathbf{W}^T\right)\\+B_{12}c_\varphi\left(\mathbf{W}^T\boldsymbol{\Phi}+\boldsymbol{\Phi}^T\mathbf{W}\right)+B_{16}c_\varphi\left(\mathbf{W}^T\frac{\partial\boldsymbol{\Phi}}{\partial\theta}+\frac{\partial\boldsymbol{\Phi}^T}{\partial\theta}\mathbf{W}\right)\\+B_{12}s_\varphi\left(\mathbf{W}^T\frac{\partial\boldsymbol{\Phi}}{\partial\varphi}+\frac{\partial\boldsymbol{\Phi}^T}{\partial\varphi}\mathbf{W}\right)+B_{12}s_\varphi c_\varphi\frac{R_\varphi}{R_0}\left(\mathbf{W}^T\boldsymbol{\Phi}+\boldsymbol{\Phi}^T\mathbf{W}\right)\\+B_{26}s_\varphi\frac{R_\varphi}{R_0}\left(\mathbf{W}^T\frac{\partial\boldsymbol{\Phi}}{\partial\theta}+\frac{\partial\boldsymbol{\Phi}^T}{\partial\theta}\mathbf{W}\right)\end{array}\right\}dS \tag{B.14}$$

$$\mathbf{K}_{w\theta}=\int\int\left\{\begin{array}{l}\kappa A_{44}R_\varphi\left(\frac{\partial\mathbf{W}^T}{\partial\theta}\boldsymbol{\Theta}+\frac{\partial\mathbf{W}}{\partial\theta}\boldsymbol{\Theta}^T\right)+B_{12}\left(\frac{\partial\boldsymbol{\Theta}^T}{\partial\theta}\mathbf{W}+\frac{\partial\boldsymbol{\Theta}}{\partial\theta}\mathbf{W}^T\right)\\+B_{16}\frac{R_0}{R_\varphi}\left(\frac{\partial\boldsymbol{\Theta}^T}{\partial\varphi}\mathbf{W}+\frac{\partial\boldsymbol{\Theta}}{\partial\varphi}\mathbf{W}^T\right)-B_{16}c_\varphi\left(\boldsymbol{\Theta}^T\mathbf{W}+\boldsymbol{\Theta}\mathbf{W}^T\right)\\+B_{22}s_\varphi\left(\frac{\partial\boldsymbol{\Theta}^T}{\partial\theta}\mathbf{W}+\frac{\partial\boldsymbol{\Theta}}{\partial\theta}\mathbf{W}^T\right)+B_{26}s_\varphi\left(\frac{\partial\boldsymbol{\Theta}^T}{\partial\varphi}\mathbf{W}+\frac{\partial\boldsymbol{\Theta}}{\partial\varphi}\mathbf{W}^T\right)\\-B_{16}c_\varphi s_\varphi\frac{R_\varphi}{R_0}\left(\boldsymbol{\Theta}^T\mathbf{W}+\boldsymbol{\Theta}\mathbf{W}^T\right)\end{array}\right\}dS \tag{B.15}$$

$$\mathbf{K}_{\varphi\varphi}=\int\int\left\{\begin{array}{l}\kappa A_{55}R_0R_\varphi\boldsymbol{\Phi}^T\boldsymbol{\Phi}+D_{11}\frac{R_0}{R_\varphi}\frac{\partial\boldsymbol{\Phi}^T}{\partial\varphi}\frac{\partial\boldsymbol{\Phi}}{\partial\varphi}+D_{22}\frac{R_\varphi}{R_0}c_\varphi^2\boldsymbol{\Phi}^T\boldsymbol{\Phi}\\+D_{66}\frac{R_\varphi}{R_0}\frac{\partial\boldsymbol{\Phi}^T}{\partial\theta}\frac{\partial\boldsymbol{\Phi}}{\partial\theta}+D_{12}\left(\frac{\partial\boldsymbol{\Phi}^T}{\partial\varphi}\boldsymbol{\Phi}+\frac{\partial\boldsymbol{\Phi}}{\partial\varphi}\boldsymbol{\Phi}^T\right)\\+D_{16}\left(\frac{\partial\boldsymbol{\Phi}^T}{\partial\varphi}\frac{\partial\boldsymbol{\Phi}}{\partial\theta}+\frac{\partial\boldsymbol{\Phi}}{\partial\varphi}\frac{\partial\boldsymbol{\Phi}^T}{\partial\theta}\right)+D_{26}\frac{R_\varphi}{R_0}c_\varphi\left(\boldsymbol{\Phi}^T\frac{\partial\boldsymbol{\Phi}}{\partial\theta}+\boldsymbol{\Phi}\frac{\partial\boldsymbol{\Phi}^T}{\partial\theta}\right)\end{array}\right\}dS \tag{B.16}$$

$$\int\int \left\{K^{\varphi}_{\varphi 0}\boldsymbol{\Phi}^T\boldsymbol{\Phi}\right\}_{|\varphi=\varphi_0} dS_0 + \int\int \left\{K^{\varphi}_{\varphi 1}\boldsymbol{\Phi}^T\boldsymbol{\Phi}\right\}_{|\varphi=\varphi_1} dS_1 + \int\int \left\{K^{\varphi}_{\theta 0}\boldsymbol{\Phi}^T\boldsymbol{\Phi}\right\}_{|\theta=0} dS_2$$
$$+\int\int \left\{K^{\varphi}_{\theta 1}\boldsymbol{\Phi}^T\boldsymbol{\Phi}\right\}_{|\theta=\phi} dS_3 + \int\int \left\{K^{\varphi}_{uc}\left(\boldsymbol{\Phi}_{|\theta=0} - \boldsymbol{\Phi}_{|\phi=2\pi}\right)^T\left(\boldsymbol{\Phi}_{|\theta=0} - \boldsymbol{\Phi}_{|\phi=2\pi}\right)\right\} dS_2$$

$$\mathbf{K}_{\varphi\theta} = \int\int \left\{\begin{array}{l} \kappa A_{45}R_0R_{\varphi}\left(\boldsymbol{\Phi}^T\boldsymbol{\Theta} + \boldsymbol{\Theta}^T\boldsymbol{\Phi}\right) + D_{12}\left(\frac{\partial\boldsymbol{\Phi}^T}{\partial\varphi}\frac{\partial\boldsymbol{\Theta}}{\partial\theta} + \frac{\partial\boldsymbol{\Phi}}{\partial\varphi}\frac{\partial\boldsymbol{\Theta}^T}{\partial\theta}\right) \\ +D_{22}\frac{R_{\varphi}}{R_0}c_{\varphi}\left(\boldsymbol{\Phi}^T\frac{\partial\boldsymbol{\Theta}}{\partial\theta} + \boldsymbol{\Phi}\frac{\partial\boldsymbol{\Theta}^T}{\partial\theta}\right) + D_{66}\left(\frac{\partial\boldsymbol{\Phi}^T}{\partial\theta}\frac{\partial\boldsymbol{\Theta}}{\partial\varphi} + \frac{\partial\boldsymbol{\Phi}}{\partial\theta}\frac{\partial\boldsymbol{\Theta}^T}{\partial\varphi}\right) \\ -D_{66}\frac{R_{\varphi}}{R_0}c_{\varphi}\left(\frac{\partial\boldsymbol{\Phi}^T}{\partial\theta}\boldsymbol{\Theta} + \frac{\partial\boldsymbol{\Phi}}{\partial\theta}\boldsymbol{\Theta}^T\right) + D_{16}\frac{R_0}{R_{\varphi}}\left(\frac{\partial\boldsymbol{\Phi}^T}{\partial\varphi}\frac{\partial\boldsymbol{\Theta}}{\partial\varphi} + \frac{\partial\boldsymbol{\Phi}}{\partial\varphi}\frac{\partial\boldsymbol{\Theta}^T}{\partial\varphi}\right) \\ -D_{16}c_{\varphi}\left(\frac{\partial\boldsymbol{\Phi}^T}{\partial\varphi}\boldsymbol{\Theta} + \frac{\partial\boldsymbol{\Phi}}{\partial\varphi}\boldsymbol{\Theta}^T\right) + D_{26}c_{\varphi}\left(\boldsymbol{\Phi}^T\frac{\partial\boldsymbol{\Theta}}{\partial\varphi} + \boldsymbol{\Phi}\frac{\partial\boldsymbol{\Theta}^T}{\partial\varphi}\right) \\ -D_{26}\frac{R_{\varphi}}{R_0}c_{\varphi}^2\left(\boldsymbol{\Phi}^T\boldsymbol{\Theta} + \boldsymbol{\Phi}\boldsymbol{\Theta}^T\right) + D_{26}\frac{R_{\varphi}}{R_0}\left(\frac{\partial\boldsymbol{\Phi}^T}{\partial\theta}\frac{\partial\boldsymbol{\Theta}}{\partial\theta} + \frac{\partial\boldsymbol{\Phi}}{\partial\theta}\frac{\partial\boldsymbol{\Theta}^T}{\partial\theta}\right) \end{array}\right\} dS \tag{B.17}$$

$$\mathbf{K}_{\theta\theta} = \int\int \left\{\begin{array}{l} \kappa A_{44}R_0R_{\varphi}\boldsymbol{\Theta}^T\boldsymbol{\Theta} + D_{22}\frac{R_{\varphi}}{R_0}\frac{\partial\boldsymbol{\Theta}^T}{\partial\theta}\frac{\partial\boldsymbol{\Theta}}{\partial\theta} \\ +D_{66}\left(\frac{R_0\partial\boldsymbol{\Theta}}{\partial\varphi} - R_{\varphi}\boldsymbol{\Theta}c_{\varphi}\right)\left(\frac{1}{R_{\varphi}}\frac{\partial\boldsymbol{\Theta}}{\partial\varphi} - \frac{1}{R_0}\boldsymbol{\Theta}c_{\varphi}\right)^T \\ +D_{26}\left(\frac{\partial\boldsymbol{\Theta}^T}{\partial\theta}\frac{\partial\boldsymbol{\Theta}}{\partial\varphi} + \frac{\partial\boldsymbol{\Theta}^T}{\partial\varphi}\frac{\partial\boldsymbol{\Theta}}{\partial\theta}\right) - D_{26}\frac{R_{\varphi}}{R_0}c_{\varphi}\left(\frac{\partial\boldsymbol{\Theta}^T}{\partial\theta}\boldsymbol{\Theta} + \boldsymbol{\Theta}^T\frac{\partial\boldsymbol{\Theta}}{\partial\theta}\right) \end{array}\right\} dS \tag{B.18}$$
$$\int\int \left\{K^{\theta}_{\varphi 0}\boldsymbol{\Theta}^T\boldsymbol{\Theta}\right\}_{|\varphi=\varphi_0} dS_0 + \int\int \left\{K^{\theta}_{\varphi 1}\boldsymbol{\Theta}^T\boldsymbol{\Theta}\right\}_{|\varphi=\varphi_1} dS_1 + \int\int \left\{K^{\theta}_{\theta 0}\boldsymbol{\Theta}^T\boldsymbol{\Theta}\right\}_{|\theta=0} dS_2$$
$$+\int\int \left\{K^{\theta}_{\theta 1}\boldsymbol{\Theta}^T\boldsymbol{\Theta}\right\}_{|\theta=\phi} dS_3 + \int\int \left\{K^{\theta}_{uc}\left(\boldsymbol{\Theta}_{|\theta=0} - \boldsymbol{\Theta}_{|\phi=2\pi}\right)^T\left(\boldsymbol{\Theta}_{|\theta=0} - \boldsymbol{\Theta}_{|\phi=2\pi}\right)\right\} dS_2$$

$$\mathbf{M}_{uu} = \int\int \left\{I_0R_{\varphi}R_0\mathbf{U}^T\mathbf{U}\right\} dS \tag{B.19}$$

$$\mathbf{M}_{w} = \int\int \left\{I_0R_{\varphi}R_0\mathbf{V}^T\mathbf{V}\right\} dS \tag{B.20}$$

$$\mathbf{M}_{ww} = \int\int \left\{I_0R_{\varphi}R_0\mathbf{W}^T\mathbf{W}\right\} dS \tag{B.21}$$

$$\mathbf{M}_{\varphi\varphi} = \int\int \left\{I_2R_{\varphi}R_0\boldsymbol{\Phi}^T\boldsymbol{\Phi}\right\} dS \tag{B.22}$$

$$\mathbf{M}_{\theta\theta} = \int\int \left\{I_2R_{\varphi}R_0\boldsymbol{\Theta}^T\boldsymbol{\Theta}\right\} dS \tag{B.23}$$

$$\mathbf{M}_{u\varphi} = \int\int \left\{I_0R_{\varphi}R_0\left(\mathbf{U}^T\boldsymbol{\Phi} + \mathbf{U}\boldsymbol{\Phi}^T\right)\right\} dS \tag{B.24}$$

$$\mathbf{M}_{v\theta} = \int\int \left\{I_0R_{\varphi}R_0\left(\mathbf{V}^T\boldsymbol{\Theta} + \mathbf{V}\boldsymbol{\Theta}^T\right)\right\} dS \tag{B.25}$$

$$\mathbf{H}_u = \left\{\begin{array}{l} A^u_{00}, A^u_{01}, \cdots, A^u_{m'0}, A^u_{m'1}, \cdots, A^u_{m'n'}, \cdots, A^u_{MN}, \\ a^1_0, \cdots, a^1_M, a^2_0, \cdots, a^2_M, b^1_0, \cdots, b^1_N, b^2_0, \cdots, b^2_N \end{array}\right\} e^{j\omega t} \tag{B.26}$$

$$\mathbf{H}_v = \left\{\begin{array}{l} B^v_{00}, B^v_{01}, \cdots, B^v_{m'0}, B^v_{m'1}, \cdots, B^v_{m'n'}, \cdots, B^v_{MN}, \\ c^1_0, \cdots, c^1_M, c^2_0, \cdots, c^2_M, d^1_0, \cdots, d^1_N, d^2_0, \cdots, d^2_N \end{array}\right\} e^{j\omega t} \tag{B.27}$$

$$\mathbf{H}_w = \left\{ \begin{matrix} C_{00}^w, C_{01}^w, \cdots, C_{m'0}^w, C_{m'1}^w, \cdots, C_{m'n'}^w, \cdots, C_{MN}^w, \\ e_0^1, \cdots, e_M^1, e_0^2, \cdots, e_M^2, f_0^1, \cdots, f_N^1, f_0^2, \cdots, f_N^2 \end{matrix} \right\} e^{j\omega t} \tag{B.28}$$

$$\mathbf{H}_\varphi = \left\{ \begin{matrix} D_{00}^\varphi, D_{01}^\varphi, \cdots, D_{m'0}^\varphi, D_{m'1}^\varphi, \cdots, D_{m'n'}^\varphi, \cdots, D_{MN}^\varphi, \\ g_0^1, \cdots, g_M^1, g_0^2, \cdots, g_M^2, h_0^1, \cdots, h_N^1, h_0^2, \cdots, h_N^2 \end{matrix} \right\} e^{j\omega t} \tag{B.29}$$

$$\mathbf{H}_{\psi\theta} = \left\{ \begin{matrix} E_{00}^\theta, E_{01}^\theta, \cdots, E_{m'0}^\theta, E_{m'1}^\theta, \cdots, E_{m'n'}^\theta, \cdots, E_{MN}^\theta, \\ k_0^1, \cdots, k_M^1, k_0^2, \cdots, k_M^2, q_0^1, \cdots, q_N^1, q_0^2, \cdots, q_N^2 \end{matrix} \right\} e^{j\omega t} \tag{B.30}$$

where

$$\mathbf{U} = \left\{ \begin{matrix} \cos\lambda_0\varphi, \cdots, \cos\lambda_0\varphi\cos\lambda_n\theta, \cdots, \cos\lambda_M\varphi\cos\lambda_N\theta, \\ \chi_1(\theta), \cdots, \chi_1(\theta)\cos\lambda_m\varphi, \cdots, \chi_2(\theta)\cos\lambda_M\varphi, \\ \zeta_1(\varphi), \cdots, \zeta_1(\varphi)\cos\lambda_m\theta, \cdots, \zeta_2(\varphi)\cos\lambda_M\theta, \end{matrix} \right\} \tag{B.31}$$

$$\mathbf{V} = \mathbf{W} = \boldsymbol{\Phi} = \boldsymbol{\Theta} = \mathbf{U} \tag{B.32}$$